Fiber Laser Welding
of
Advanced High Strength Steels

by

Daniel Westerbaan

A thesis
presented to the University of Waterloo
in fulfillment of the
thesis requirement for the degree of
Master of Applied Science
in
Mechanical Engineering

Waterloo, Ontario, Canada, 2013

Authors Declaration

I hereby declare that I am the sole author of this thesis. This is a true copy of the thesis, including any required final revisions, as accepted by my examiners.

I understand that my thesis may be made electronically available to the public.

Abstract

Fiber laser welding (FLW) was used to join advanced high strength steel (AHSS) and high strength steel (HSS); specifically two dual-phase (DP) steels, with ultimate tensile strengths above 980 MPa and with different chemistries (DP980 Rich and DP980 Lean), and a high strength low alloy (HSLA) steel, with an ultimate tensile strength of 450MPa (HSLA450). The welding speed and power were varied to develop a process envelope for minimizing weld concavity. In order to attain welds free of weld concavity a balance of speed and power was required; weld concavity could be reduced by lowering power and increasing speed. Welds with amounts of concavity ranging from 15 % to 35 % were characterized with respect to hardness, tensile and fatigue testing. Tensile results revealed that DP steel was sensitive to weld concavity while HSLA450 was not. At stress amplitudes enduring beyond 1000 cycles, welded specimens exhibited lower fatigue resistance compared to the base metal. Concavity reduced the fatigue life of DP980 steels, where increasing the amount of concavity further reduced the fatigue resistance, while the fatigue resistance of HSLA steel welds was not sensitive to weld concavity.

Hardness profiling of the welds revealed that HAZ softening was present in the DP980 steel welds. The amount of HAZ softening was normalized; allowing for comparison of different steels. Welds made by FLW demonstrated reduced softening compared other laser welding types because FLW was capable of welding with lower heat input.

A difference in the FZ hardness was observed between the DP980 steels because of the difference in carbon content of the steels; where higher carbon content resulted in higher FZ hardness. Additionally the high cooling rate in FLW created higher fusion zone hardness than the values predicted by Yurioka's model based on arc welding.

Examination of the microstructure revealed that the soft zone of DP980 Lean steel possessed severely tempered martensite and untransformed ferrite while DP980 Rich generated a structure with a mixture of tempered martensite, untransformed ferrite and a small fraction of non-tempered martensite. This difference in HAZ softening was attributed to the alloying content of the DP980 Rich steel the higher alloying content of DP980 Rich steel formed a stable austenite that could exist near the Ac_1 temperature and enabled the formation of new martensite in the soft zone.

The effects of HAZ softening were apparent in tensile testing where the DP980 Lean steel, which exhibited higher softening, demonstrated by a severe reduction in elongation while the DP980 Rich steel, which had higher resistance to softening, attained elongation comparable to its base metal. HSLA450 exhibited a slight reduction in elongation due to the hardening of the fusion zone. The welded DP980 Rich and HSLA450 steels consistently failed within the base metal, while the DP980 Lean steel failed in the soft zone.

The welded DP980 Rich steel also demonstrated limiting dome heights comparable to the base metal while the severe softening in the DP980 Lean led to premature fracture in the soft zone, yielding a larger reduction in the limiting dome height.

Acknowledgements

Unfortunately, I will not be capable of listing every individual who has assisted and aided me over these last two years, but I will try. Please note that I truly appreciate and value the support I have received from colleagues, friends and family and if you feel you have been overlooked in this list, please know that you have not been forgotten.

This research project (and the rest of CAMJ for that matter) would not exist without the dedicated support of my supervisor, Dr. Norman Zhou. Dr. Zhou has balanced the difficult task of guiding students while allowing them independence to pursue their own research objectives and because of his efforts, my time at CAMJ has been rewarding in meeting research objectives as well as developing a deeper understanding of laser welding.

I would also like to thank and acknowledge Mr. Elliot Biro, of Arcelor-Mittal Dofasco, for his discussions, comments and time; all of which proved invaluable to furthering the work as well as my own understanding. I also wish to extend gratitude to the research and development team at Arcelor-Mittal Dofasco for their hospitality, accommodations and fellowship during many visits to the numerous "greasy spoon" establishments of Hamilton ON.

It should go without saying that Dr. Sashank Nayak was instrumental in completing the work his kindness, calm-demeanor and patience are traits that will assist him wherever he goes.

Mr. Dulal Saha has demonstrated a pleasant eagerness to assist within this work. His readiness to share in laboratory management, emails sending relevant papers and genuine interest in the research has benefitted not only my own self, but all of CAMJ as well.

The helpful discussion and dedicated efforts of Mr. Dennis Parkes, Mr. Raymond Xu and Dr. Daolun Chen greatly helped in furthering our understanding of laser welded blanks; it was also a joy to meet and visit with Mr. Parkes exploring many of Toronto's fine dining establishments.

Mr. Frank Goodwin and the International lead zinc research organization are also gratefully acknowledged for their financial support. Mr. Goodwin's kind demeanor and hospitality made each of the GAP presentations a joy to attend.

...to the almighty and living God

Table of Contents

List of Figures

List of Tables

Chapter 1: Introduction

1.1   Overview

Advanced high strength Steels (AHSS) are widely used in the automotive industry as a means to reduce vehicle weight while maintaining stringent crash test standards, as such there is a need to understand the weldability of these alloys. Furthermore the application of laser welded blanks (LWB), also known as tailor welded blanks, are increasingly used to join materials which are then formed via pressing operations. In recent years fiber laser welding (FLW) has emerged as a promising technology for application in welding and has begun to emerge within industry. Therefore understanding of laser welded blanks made with advanced high strength steels via fiber laser welding is an essential research area for the automotive industry.

1.2   Justification and Problem

Government regulations are increasing both fuel efficiency and safety standards [1]. Application of high strength steel is the most cost effective solution for weight reduction at $1.02/kg [2]. Additionally, global demand for vehicles is predicted to increase by 40% from 2010 to 2018 [3]. In addition to this increase in demand, the automotive industry is moving to fewer platforms; building more models from a single body structure [4]. This further compounds the need to increase production capabilities as vehicles will share more components within the body and chassis structure [4]. The weight saving, cost effectiveness and high production capabilities of LWBs of AHSS made by FLW are an attractive option for use in the construction and manufacture of automotive body and chassis.

Current literature of FLW has focused mostly on welding of thick plate steel for use in pipeline and heavy industry applications [5, 6], while the application of FLW to the welding of thin galvanized sheet of AHSS is scarce. Additionally reported welding speeds of thin sheet using CO_2 and Nd:YAG laser welding are lower than that capable by FLW. Thus there exists the need to evaluate the weldability of thin gauge AHSS for use in LWB made by the FLW process.

1.3 Objective

The objective of this thesis is to study the FLW of AHSS by examining the processing, microstructure and mechanical properties of the welded steel sheets. Specifically the objectives include:

1. Characterization of the microstructure of FLW AHSS made at high welding speeds

2. Comparison of mechanical properties including tensile strength, formability and fatigue strengths.

3. Evaluation of the effects of weld concavity on the mechanical properties of the weldments

4. Comparison of weldability of similar grade AHSS with varied alloy content

1.4 Criteria and Constraints

Laser welding is an established industrial practice, however FLW is a relatively new welding practice as such existing standards for Nd:YAG and CO_2 laser welding, such as GM4485, are extrapolated to this work. Several standards exist for materials testing; in this study ASTM standards are applied for evaluation of the mechanical properties.

This study is limited to the joining of three materials, two AHSS and one HSS for reference, in similar combinations while the material thickness was held constant at 1.2 mm thick.

2

1.5   Outline of Thesis

In this thesis Chapter 2 outlines the various laser welding processes and presents a review of the literature on topics relevant to laser welding of AHSS. Chapter 3 describes the laboratory set up and experimental procedures followed for characterizing the welds. Chapter 4 reports on the fatigue and tensile performance of weldments possessing up to 35 % concavity for both AHSS and HSS steels. In Chapter 5 the microstructure and mechanical strength of the AHSS are reported, additionally the amount of HAZ softening made by other laser welding processes are compared to FLW. Furthermore Chapter 5 also compares the effects of alloying addition on the weldability of the two DP steels investigated. Finally the major conclusions drawn from the results of this thesis study are concluded in Chapter 6.

Chapter 2: Literature Review

2.1   Laser Welding/Process

2.1.1   Introduction

Laser stands for Light Amplification Stimulated by the Emission of Radiation [7]. A laser is generated by exciting a medium, which then radiates a photon [7]. When the medium is excited it enters a higher energy level, in order to return to its former more stable state it releases a photon while returning to the lower energy state (Figure 1) [7, 8]. The photons released travel in all directions (non-coherently), however if the released photon collides with another ion, it will release a photon which will travel with the former photon, in phase [7]. As more collisions take place the density of the in-phase photons increases [7].
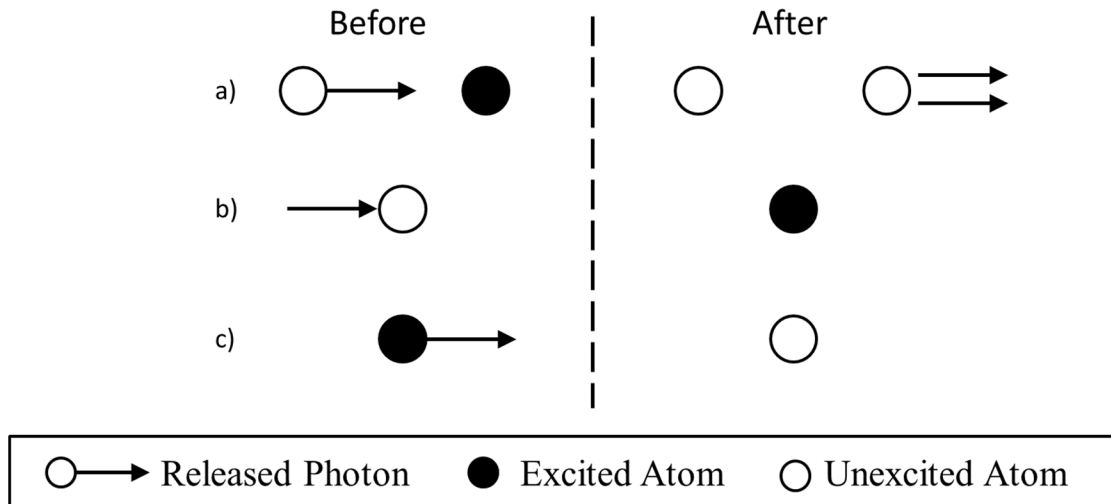
Figure 1: Stimulated emission a) release of photon from excited state by passing photon b) absorption of photon to high energy state c) release of photon to low energy state

A laser beam is a collimated beam of light which is in phase and of one wavelength [7]. To generate such a desired beam a medium is elongated in the direction of desired optical

4

transmission and placed between 2 mirrors [7]. One mirror is fully reflecting, while the other is partially reflecting. These mirrors are designed to align the wavelength of the excited photons and only allow a portion of the excited photons to be transmitted [7]. Photons travelling in directions other than along the optical axis are quickly lost from the system [7]. Reflections from the mirrors greatly increases the length travelled by photons moving parallel to the optical axis [7]. A portion of this laser is transmitted through the partially reflecting mirror [7], developing a coherent collimated beam of light as illustrated by Figure 2.
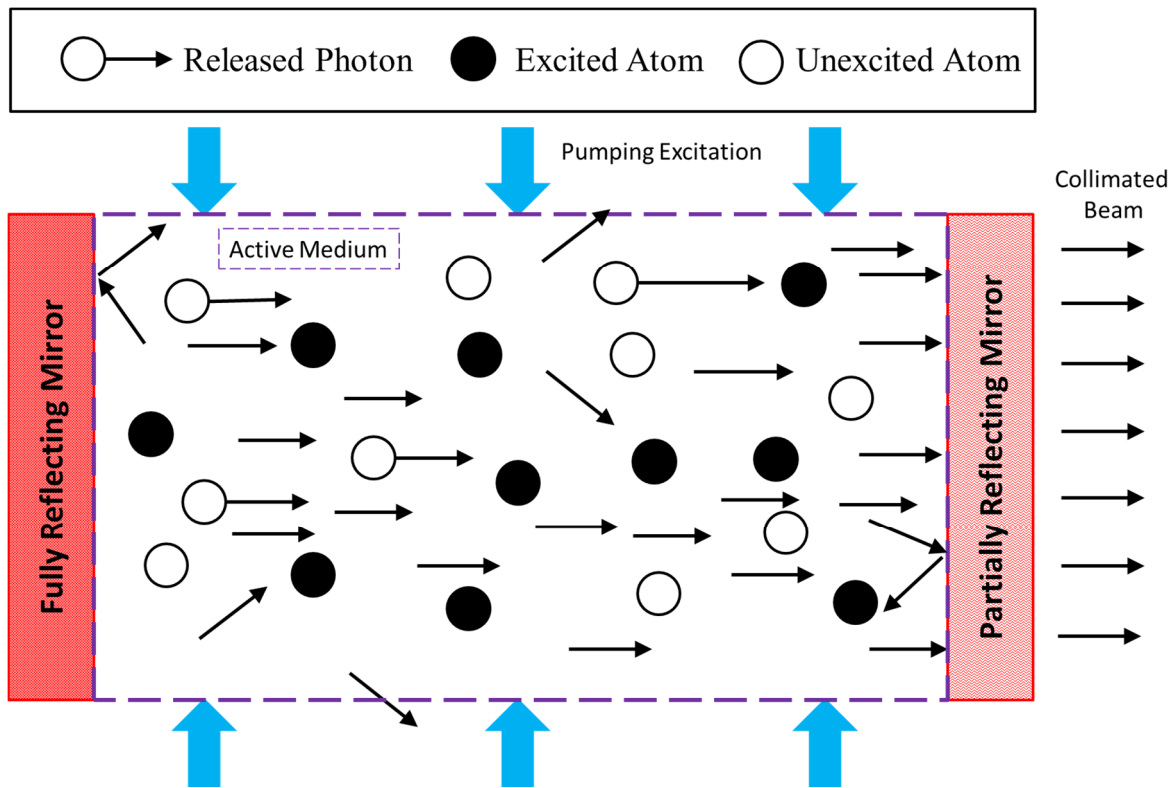
Figure 2: Basic laser operation through stimulated emission

Lasers have been applied for use in applications to measurement and instrumentation, communications and ranging, as well as biological and medical applications [9]. Report of Laser emission began in the early 1960's and as the availability of lasers increased its application for

5

use in welding and joining began being researched [10]. Thus, laser welding is a newer technology compared to other existing types of welding processes e.g. resistance spot welding and arc welding.

2.1.2 Laser Welding

Fusion welding requires the balance of heating and cooling a volume of material such that a molten liquid pool is formed that remains stable until it solidifies while the system is propagated along the interface of two solid pieces eliminating the previous seam between the two pieces as the weld pool solidifies [10]. Laser welding applies a laser as the heat source for this operation. Heat is input to the system by the adsorption of laser radiation by the metal, while heat is output from the system via uniform distribution of heat within the work piece [10].

There are two main modes of welding, keyhole mode welding and conduction mode welding [10]; illustrated in Figure 3.
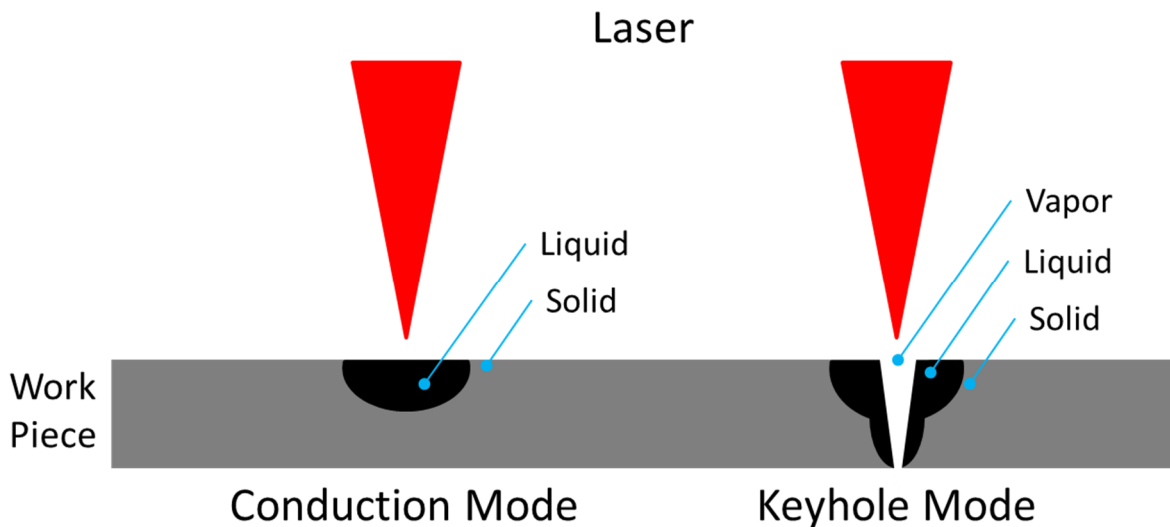
Figure 3: Conduction vs. keyhole mode welding

Conduction mode welding does not vaporize the material being joined, while keyhole mode welding forms a narrow vapor column which separates the weld pool [10]. Keyhole mode welding is capable of transferring more heat into the system, due to the higher absorption of heat from the laser beam by the vapor column [10, 11], and thus is capable of attaining higher welding speeds. Evaporation of steel, and thus keyhole formation, begins at a power intensity in the order of 10^3 W/mm^2 [7], at power intensities between 10^4 and 10^5 W/mm^2 the weld penetration greatly increases, forming narrow but deep welds while allowing for high welding speeds [7]. In excess of 10^5 W/mm^2 expulsion of liquid and evaporated metal begins [7]. This narrow cylindrical column of vapor, formed by the high heat intensity, is known as the keyhole [7].

The energy flow of the laser radiation is often interrupted because metal vapors are created from the intense heat. The hot gases often turn into plasma, severely altering the adsorption and scattering of the laser beam [10] the increase in absorption occurs as the keyhole acts like a black body [12]. The constant removal of heat from the system requires a stable geometry of the solid-liquid interface [10]. Difficulties occur in maintaining a stable geometry due to fluctuations introduced with a moving laser source [10], mainly fluctuations in laser output power and changes in the workpiece, with changes in the workpiece being the dominant source of fluctuation [10].

As research continued new lasers, including solid state and gas state lasers, were developed such as Nd:YAG and CO_2 [8, 10]. Additionally, solid state array (diode) lasers have been developed as well [8, 10] while more recently the emergence of fiber lasers as an industrial application has gained interest [13].

2.1.3   Laser Welding Types

CO$_2$ Lasers

CO$_2$ lasers use gas, (CO$_2$) as the medium for excitation and emission of photons. CO$_2$ lasers are capable of high average powers and therefore high welding speeds and penetration depths [7]. However, CO$_2$ lasers require a hard interface beam delivery [10, 14], that is a series of fixed mirrors and lenses are used to move the beam from the source where it is desired to weld [10]. Thus beam delivery of CO$_2$ lasers can be complex and challenging in industrial applications. In addition to beam delivery CO$_2$ lasers possess a large footprint due to chiller size requirements [14]. Additionally CO$_2$ laser welders have higher maintenance demands, from the fixed optics [13] as well as the higher operation cost due to He shielding gas requirements and poor system efficiencies [13].

Nd:YAG Lasers

Nd:YAG laser systems utilize a Neodymium doped Ytterbium Aluminum Garnet crystal as the medium for excitation. Nd:YAG lasers operate in both pulsed and continuous wave (CW) modes where the beam is controlled to provide a fluctuating source to a constant power output [10]. Typical wavelength of the emitted photon is in the range of 1.06 µm making it possible for transmission of the beam through fiber-optic cables [7, 10]. To attain higher average power the beam is pulsed [7] which in turn allow for higher welding speeds, or the ability to attain greater penetration [7]. One disadvantage of Nd:YAG lasers is the lower energy efficiencies attained compared to other lasers [14].

Diode Lasers

Diode Lasers or high powered diode lasers (HPDLs) are newer than traditional forms of laser welding (such as Nd:YAG and CO_2). HPDLs harness an array of diodes as a light emission source and have been implemented for use in welding since the mid 1990's [15]. HPDLs utilize semiconductors as the active medium with AlGaAs as the most common medium, with wavelengths within the range of 800-810 nm [16, 17]. For the necessity to cool the diodes, the diodes are assembled in thin strips which are subsequently mounted to a heat sink, [18]. Due to this arrangement, the optical emission diverges in the plane of the thin strip leading to the formation of an elliptical beam [18]. Furthermore, this divergence is compounded when the thin strips are assembled into an array of diodes, to provide enough power for welding [18]; thus, HPDLs possess poorer beam quality than other welds [17] and from the lower power density are only capable to perform conduction mode welding.

Fiber Lasers

Fiber lasers technology has been demonstrated since the 1960's [19]. However, fiber lasers have only gained interest recently for application in welding due to the recent improvements in grating technology and increases in power operation [13]. For the excitation source fiber lasers use an ytterbium doped core, which is activated by diode pumps [13]; these systems are then bundled together to provide higher powers. The competitive cost of fiber lasers [13, 20] may eventually lead to the displacement of Nd:YAG systems [13]. Among all laser welding processes, fiber laser welding offers higher welding speed because of the higher beam quality [13]. The increased ease of operation, and lower energy consumption [13], makes FLW an attractive industrial application and is as such an important laser welding process for research.

2.2 Welding Parameters

The beam type and quality are not the only factors affecting a welds capability in a given situation. Optimum welding parameters are generally determined by a trial and error method in which weld parameters are varied and with the results recorded to develop guidelines for welds which generally lead to acceptable welds [10]. The main process parameters that must be considered for laser welding are those which affect the amount of heat transferred to the work piece, as such it is the materials, the power intensity and time given for the material to absorb heat [7, 10]. Thus the main variables include: the material being joined; its coating type, absorption and reflectivity, as well as the heat input applied to the material; its net power, spot size, focal depth, while the time for heat transfer is mostly dictated by the welding speed.

Generally, power determines the penetration depth for a given welding speed [10], this relation is closely related to the welding speed, along with the material absorption of the laser beam these parameters determine the amount of energy input to the system [10]

2.3 Laser welded blanks

To reduce vehicle weight it was actually the steel industry, in efforts to remain competitive with arising technologies such as aluminum, that greatly pushed for the development of the laser welded blank (LWB), also known as tailor welded blanks, [7], [21]. The manufacturing of LWBs involves butt welding two pieces, of either similar or different combinations of gauge or composition, which are then pressed to form a complex geometry [10, 21-23]. Weight and cost savings can be attained by optimizing the gauge thickness and material grade by using thicker or stronger material where necessary and joining to a thinner or cheaper material where strength is not necessary [10]. Additionally, the amount of waste generated can be reduced by proper design

of the blanks [7] as well as by carefully nesting smaller pieces within the holes of larger ones, during the initial cutting of the steel coil [10]. Deep drawing capabilities and high formability is required of a tailor blanks, which is then required of the weld as well [10]. Thus the weld must possess good ductility [7]. To prevent damage or excessive wear to the die tooling the weld bead needs to be flush with the joined sheet [7].To maintain the corrosion resistance of galvanized sheets the heat affected zone (HAZ) must be narrow [10], preserving the cathodic protection of the zinc. Also, the welded blank must possess tight dimensional tolerance so it can be repeatedly loaded into the forming tools and produce consistent geometries; the welding process must provide low heat input to minimize the effects of thermal distortion [21]. Thus, the narrow HAZ, low distortion and high welding speed makes laser welding attractive for the assembly and construction of components for use in automotive chassis, and body structures [7, 10, 21].

Previous attempts by Honda Inc. in 1976 to make tailored blanks were unsuccessful due to the high thermal distortion of the TIG welding process used [21]; however, the first successful commercial application of tailor blanks in the automotive industry was by Thyssen-Stahl [7, 21] with the development of a floor pan for the Audi A100 in 1985 [21]. Initially it was desired to make the floor plan from a single piece 1960 x 3200 x 0.75 mm however, at the time there, was no capability to make galvanized steel sheet of this size [7], so it was decided that two pieces would be joined together to form one of the required dimensions; while the only joining process capable of meeting the aforementioned requirements was laser welding [7, 21] leading to the development of the laser welded blank (LWB) which is extensively used in the automotive industry to this day [3, 22-23]

To join two materials, LWBs utilize a butt joint design which is one of the most difficult joints to make via laser welding as the small spot size and high welding speed leave little tolerance for the

11

beam to leave to joint seam [7, 24], requiring tight fit up and edge preparation of the work pieces [10]. As welding speed increases, or the part thickness decreases, the requirements for good joint fit up increases [7] e.g. when welding thin sheet, to ensure sufficient material is melted by the laser beam which then flows to bridge any gap between the sheets and solidifies to form a joint, gaps between the work pieces must be less than 0.1mm [7, 10] or half the laser spot size [7], whichever is less. In general LWBs are commonly made up of mild steel or IF steel; however, the weight reduction capabilities of the LWBs has been reported to increase by using high strength steel (HSS) and advanced high strength steel (AHSS) [25-27].

2.3.1   High Strength Low Alloy (HSLA) Steel

HSLA steels utilize small amounts of alloying addition, and are strengthened by the fine ferrite matrix, solid solution hardening and precipitation hardening [22, 28]. The fine ferrite matrix is formed by the control of the austenite grain size through the formation of fine precipitates (carbides, carbon-nitrides and nitrides) during hot rolling which prevent grain growth by pinning the grain boundaries [28]. As it is possible to control the formation of the precipitates through micro alloying with 0.1wt-% of elements such as Nb, Ti, or V, HSLA steels possess lower carbon content and thus attain good weldability [28]. HSLA steels possess both high ductility and strength; this makes HSLA suitable for automotive applications that require deep drawing capabilities such as tailored blanks [28]. A typical HSLA microstructure is shown in Figure 4 with fine grained ferrite (dark regions) strengthened by carbides (bright spots).
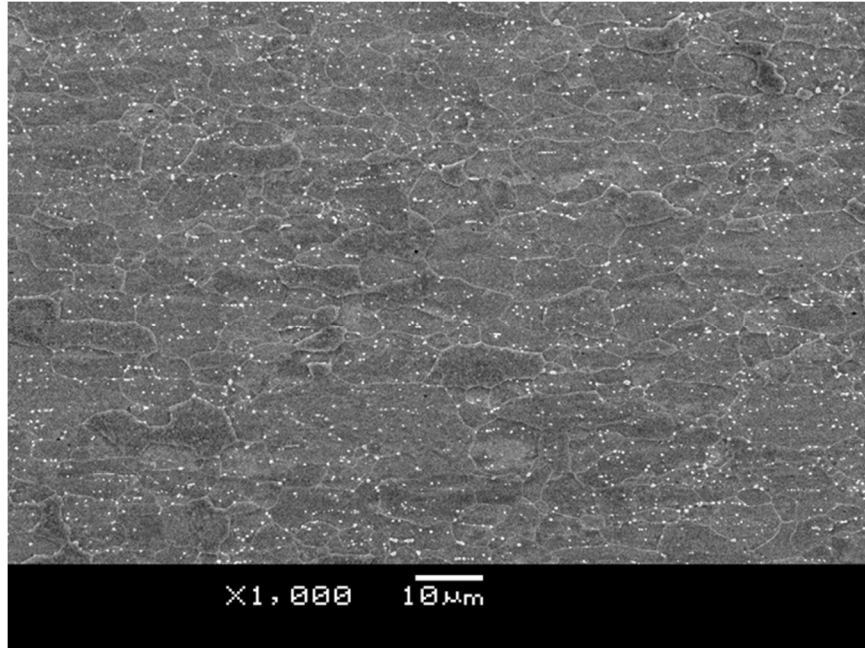
Figure 4: HSLA microstructure

2.4 Advanced High Strength Steel

In effort to meet the automotive industry's demand for weight reduction with high formability and competitive cost steel makers have developed high strength steel (HSS) and advanced high strength steel (AHSS). The different mechanical properties are attained by controlling the cooling rate from the austenite (or ferrite-austenite phase; depending on alloying addition) to stable and/or metastable phases at room temperature [22]. Additionally, rolling operations may also be performed to manipulate grain structure and size. The many types of advanced high strength steels include, interstitial free (IF), high strength low alloy (HSLA), bake hardened (BH), dual-phase (DP), transformation induced plasticity (TRIP), twinning induced plasticity (TWIP), and martensitic (MS) steels. Within a type of steel there is a large variation in the strength which can be attained see Figure 5.
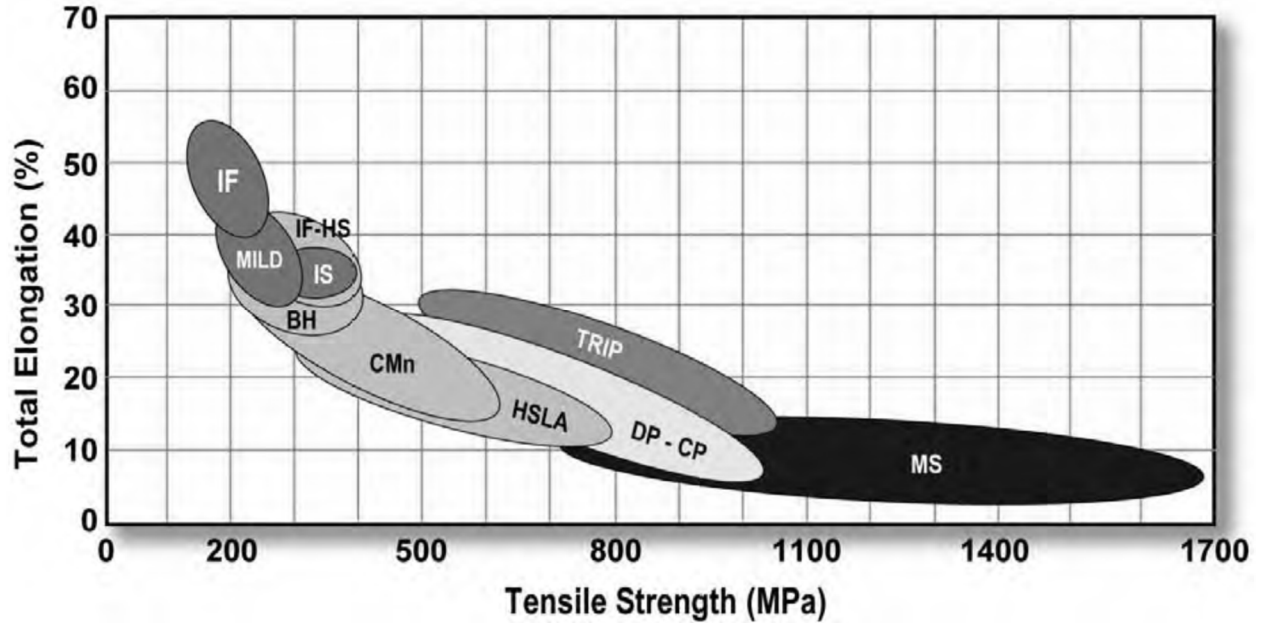
Figure 5: Strength and elongations attained by AHSS [22]

In order to distinguish between the many types of steels auto and steel makers have developed a system to identify steel by both their microstructure and their ultimate tensile strength, e.g. dual phase steel with an ultimate tensile strength of 600 MPa would be referred to as DP600.

2.4.1 DP Steel

DP steels are comprised of a ferrite matrix with martensite islands dispersed throughout [22, 28-29]. DP steel is formed by inter-critical annealing where a portion of the austenite phase is transformed to ferrite, and then upon rapid cooling the remaining austenite is transformed to martensite [22, 28]. DP steels attain the necessary hardenability through increased carbon content and alloying additions [28]. The martensitic phase causes strain to be concentrated in the ferrite, creating a high work hardening rate [22], this high work hardening rate increases the energy absorption characteristics, making DP steel suitable candidates for use in automotive chassis [28]. Typical DP microstructure is shown in Figure 6 with ferrite matrix (dark regions) and martensite stringers (bright regions).

14
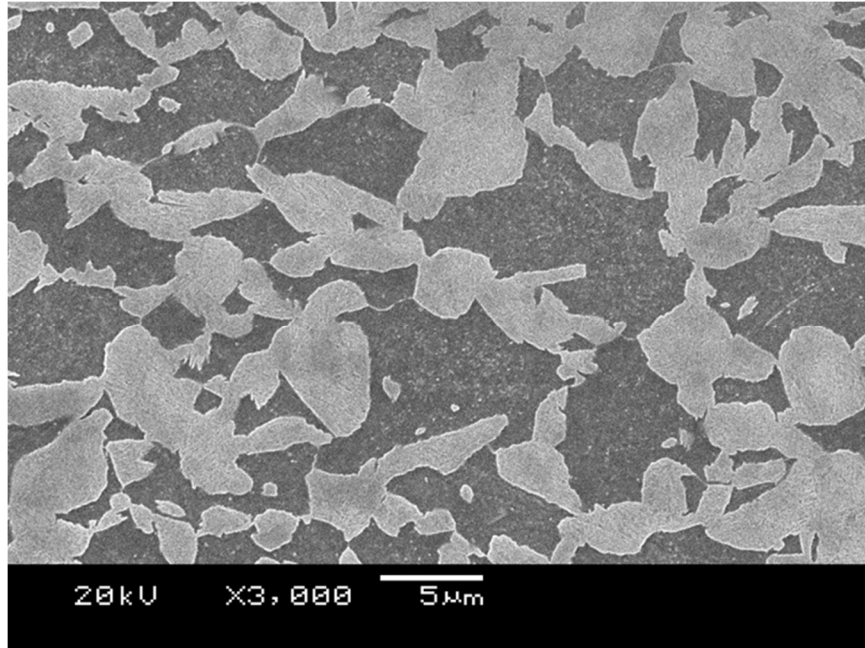
Figure 6: Dual phase steel microstructure

2.5 Solidification of the weld pool

This section outlines basic solidification concepts steel and how they apply to laser welding. Essentially welding is simply the melting and solidification of steel, but at a much higher heating and cooling rate compared to steel manufacturing. Laser welding in particular exhibits very high heating and cooling rates, as such this section has been tailored to address solidification concepts at these higher rates.

2.5.1 Nucleation

As the heat source is removed, and the temperature falls below the melting temperature, the liquid becomes thermodynamically unstable, leading to the nucleation of the solid phase [28, 30]. However, the energy required to start solidification is much less on an existing solid or nuclei [28, 30], thus in welding, solidification begins as the solid-liquid boundary of the weld pool [8].

15

2.5.2   Growth

Liquid grows from existing grains of the BM according to epitaxial growth [8]. Then competitive

growth occurs as solidification continues in the direction of maximum temperature gradient [8].

Furthermore at high welding speeds, there is enough undercooling for the nucleation of a fine

grained equiaxed structure in the FZ [8], as shown in Figure 7.
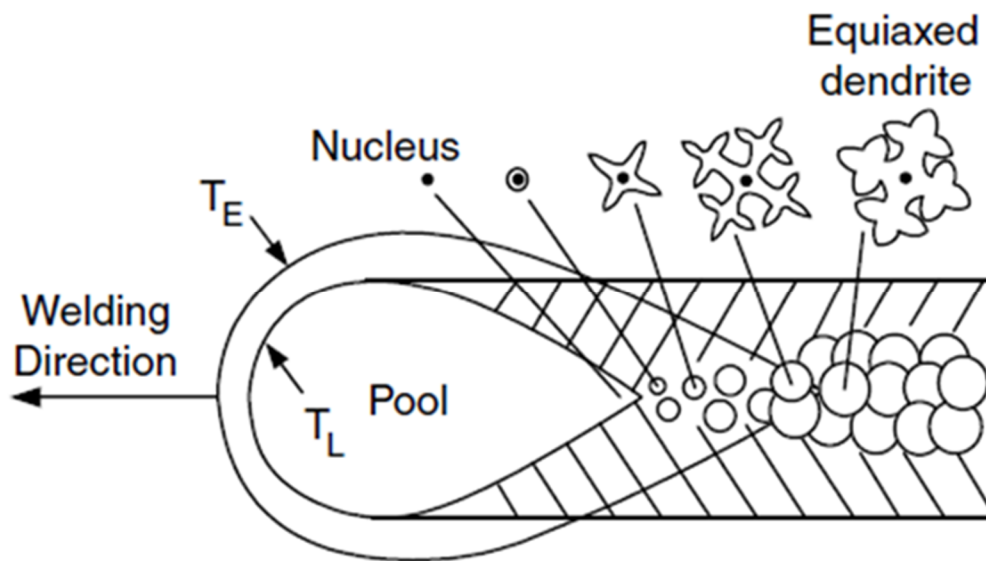
Figure 7: Solidification of weld pool in high speed welds [8]

2.5.3   Phase Transformations

The Fe-C Phase Diagram

In steels the solid particles form into different crystallographic structures according to their alloy

content, which is represented via the phase diagram Figure 8. The Fe-C phase diagram depicts

the structure which will form under equilibrium conditions. Under these conditions steels

containing less than 0.65 % carbon (common amongst most automotive steels) will solidify and

form austenite, upon further cooling the steel undergoes a solid state transformation, where FCC

16

austenite transforms to BCC ferrite. Once the solid cools to the eutectic temperature (727°C) the remaining austenite transforms to pearlite, a lamellar structure of ferrite and cementite. However, when the cooling rate is high, such as in welding, equilibrium conditions cannot be met which leads to a change in the transformation kinetics; the transformation temperatures become altered from those predicted by the phase diagram and other microstructures, such as martensite and bainite can form.
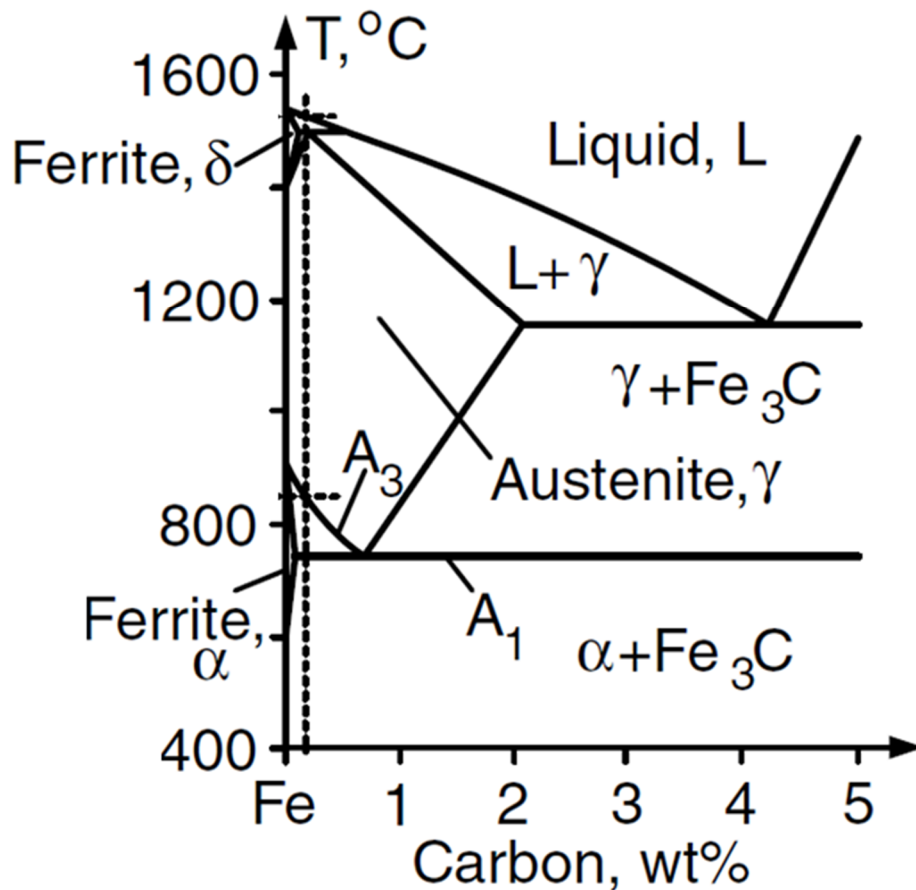
Figure 8: Fe-C phase diagram [8]

A useful tool for analyzing the non-equilibrium cooling conditions is the continuous cooling transformation (CCT) curve. CCT curves show the transformation products for a given alloy

17

composition, cooled at a constant rate over a given period of time. Figure 9 shows a typical CCT diagram for steel, it should be noted that as cooling rates increase martensite and bainite may be formed.
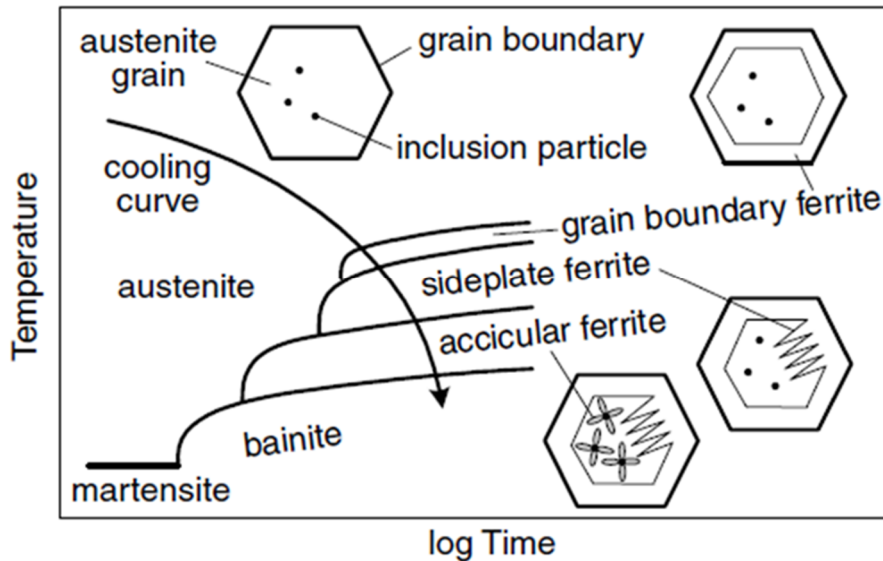
Figure 9: Typical CCT diagram for carbon steels [8]

Martensite Formation

Martensite is a lathy, or needle like, structure developed by rapid cooling in carbon steels [28, 30-31]. The morphology of martensite depends on the carbon content: martensite exhibits a lath like morphology in steel containing lower carbon contents (less than 0.5 wt-% C) [32]. Lath type martensite is dominant in low carbon steels while plate martensite occurs in medium and high carbon steels [30]. While, plate type martensite forms between 0.5 to 1.4 wt-% C and martensite twins form when carbon content exceeds 1.4 wt-% [32]. In general, martensite is hard and strengthens the material greatly, however behaves in a brittle manner [28, 30-31]. Martensite is formed via diffusionless transformation of the austenite phase [28, 30-31]. When there is not

18

sufficient time for carbon to move from interstitial sites of the FCC structure the carbon atoms get trapped during the transformation [31], which causes twinning of the lattice [30] that forms a body centered tetragonal (BCT) structure [31]. Once this nucleation begins it grows independent of thermal activation [30, 31] at speeds approaching the speed of sound in the material until impeded by a barrier such as a grain boundary or another martensite lath [30].

Bainite Formation

Bainite is a mixture of ferrite and carbides, which form due to large under cooling below the nose of the pearlite transformation curve [30]. Bainite is obtained at transformation temperatures where the ferrite transformation is sluggish as well as at temperatures below the martensite start temperature [33]. Bainite growth occurs in two stages; first ferrite grows, then carbides precipitate [33]. Commonly two types of bainite are formed in steel; upper bainite comprising of sheaves of ferrite plates with cementite particles between the plates (forms at higher temperature 350-450°C) while lower bainite, which forms below 350°C, consists of fine cementite particles precipitated within bainitic-ferrite plates or laths [33].

Factors affecting microstructure formation

Microstructures that form by rapid cooling depend on the grain size and the cooling rate [30]. Also, different alloying additions shift the curves of the CCT diagram, increasing the hardenability of the steel; allowing for easier formation of martensite [8, 28, 30]. Elements such as Cr, Mo and Si are ferrite stabilizers; that is they shift the nose of the CCT curve to shorter transformation times for the formation of ferrite or pearlite while elements such as Ni, Mn, and Cu are austenite stabilizers; increasing the time available for transformations [30]. Additionally, reducing the austenite grain size has the effect of shifting the CCT curves to shorter transformation times [8, 30]; making it harder to form martensite.

2.5.4   Weld zones & Microstructures

The microstructures observed in welding can be readily correlated to the Fe-C phase diagram as shown in Figure 10.
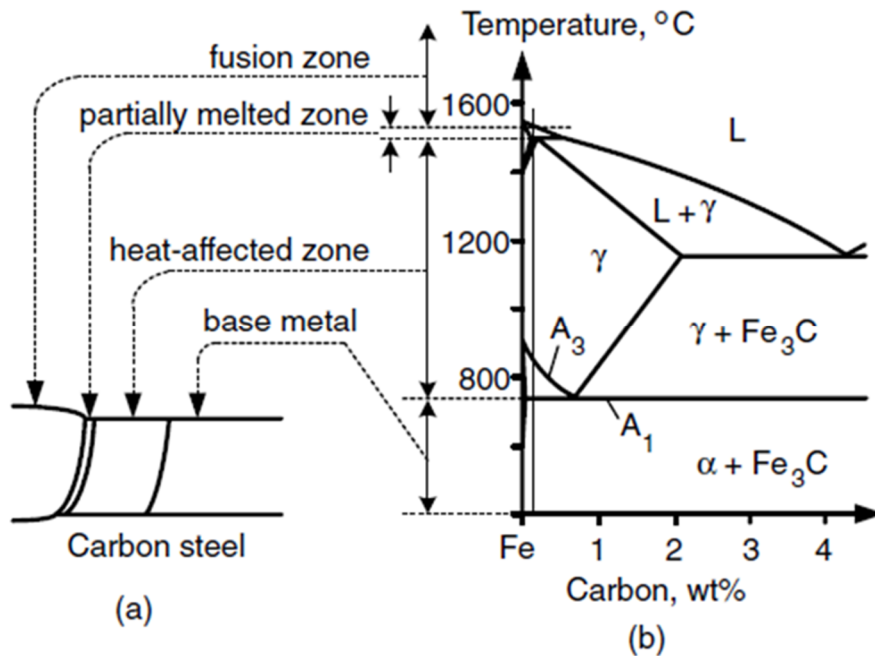
Figure 10: Correlation of transformation temperatures to weld zones: (a) weld zones (b) Fe-C phase diagram [8]

Fusion Zone

The fusion zone (FZ) corresponds to the area of the weld which exceeds the liquidus temperature. This area cools through the freezing point to solidify into austenite; upon cooling past the A_{C1} temperature it undergoes a solid state transformation [8], which during the high cooling rates of welding usually yields martensite.

Heat affected zone

The heat affected zone (HAZ) corresponds to the area in the weld which exceeds the A_{C1} temperature but remains below the peritectic temperature. HAZ microstructures are typically those formed by rapid cooling from austenitic phases [8] additionally the high peak temperatures of welding can lead to grain growth in the HAZ [8].

2.5.5   Heat input of Laser Welding

To effectively compare changes of speed and power in addition to changes in power intensity from different laser types to the mechanical properties of the weld, the heat input to the steel sheets was calculated. The heat input was calculated using a method proposed by Xia *et al.* [34] based on the Rosenthal equation for a 2-D line source, which calculates the energy absorbed by the sheet by measuring the distance between the fusion boundary and the A_{c1} isotherm as given in Equation 1,

$$\frac{Q_{net}}{vd} = \frac{\rho c (r_{Ac1} - r_m)(2\pi e)^{\frac{1}{2}}}{\left(\frac{1}{T_{Ac1} - T_0} - \frac{1}{T_m - T_0}\right)}$$

(1)

where ⸺ is heat input (the normalized net absorbed energy per unit length),   is the distance from the weld centerline to the A_{c1} isotherm,   is the distance from the weld centerline to the fusion boundary,   is the A_{c1} temperature,   is the melting temperature,   is the room temperature,   the material density (7860 kg/m^3),   the specific heat capacity of steel (680 J/kgK) and λ the thermal conductivity (30W/m/K) [34]. The melting temperature and A_{c1}

21

temperature can be calculated using the Schürmann and Andrew's methods, respectively [35], [36].

From this heat input the time at which the material was held neat the Ac1 temperature may be calculated by:

$$\tau = \frac{1}{4\pi e \lambda \rho c} \frac{(Q_{net}/vd)^2}{(T_{Ac1} - T_0)^2}$$
(2)

Where τ is the amount of time taken to heat the sample to the Ac_1 temperature. The time constant, τ, is used to compare the time available for tempering of the martensitic phases, within the soft zone of welded DP steels, made different welding processes or different combinations of welding parameters.

2.6   Challenges in Laser Welding of AHSS

2.6.1   HAZ Softening of DP Steels

HAZ softening is an important issue in DP steels, which is still not fully understood and being investigated [34, 37]. HAZ softening is formed when the martensitic phase within the sub-critical HAZ is decomposed creating a region of tempered martensite leading to a drop in hardness below that of the BM. Earlier studies on DP980 using diode and Nd:YAG laser welding processes have revealed that tempering of the martensite in the HAZ of the weldment has a detrimental effects on the mechanical properties of the joint [34]. HAZ softening was observed to be proportional to the martensite content of the material [34]. The severity of the HAZ softening is a function of heat input, reducing heat input by increasing the welding speed, at constant power, leads to a narrower HAZ and less softening [34]. Xia *et al.* also observed that the

22

high heat input diode laser welding was found to possess the widest HAZ and most severe softening effect while softening in Nd:YAG welds was less severe, as the Nd:YAG process could weld at a lower heat input.

HAZ softening reduces the tensile strength and the fatigue life of the DP steel welds [38-42]. It has also been reported that increasing welding speed reduces softening resulting in welds with tensile strength close to that of the BM [43]. Fiber laser welding (FLW) is capable to weld at high speed and therefore is beneficial for making LWBs [13, 20-21, 44]. Furthermore, it should be noted that both concavity and HAZ softening was detrimental to the fatigue life of the DP steel welds [38-42, 45].

The HAZ softening effect has been shown to reduce the formability of the welded steel, the greater the softening effect the greater the reduction in formability [43, 46]. It was also demonstrated that by increasing HAZ width by increasing the heat input the material strength was further reduced [43].

It has also been observed that additions of Cr and Mn in the BM stabilize the martensite phase lowering the effect of softening [47] while other studies have also shown that Mo also stabilizes the martensitic phase [37]. These elements are carbide forming elements and impeded the diffusion of carbon, delaying the transformation of the martensitic phase [8].

Furthermore, studies have predicted that as the heat input was reduced the amount of softening would become negligible, leading to mechanical properties closer to that of the BM [46].

In order to effectively compare the effects of HAZ softening between different alloys and grades of DP steels the HAZ softening is normalized using the method outlined by Biro *et.al* [37] to compare the welded steel to both the BM and the fully tempered BM, as shown in Equation 3:

$$Normalized\ Softening = \frac{H_{BM} - H_{HAZ}}{H_{BM} - H_{TMP}}$$

(3)

Where the normalized softening, ranges from 0 (no tempering) to 1 (fully tempered), H_{BM} is the hardness of the unaffected BM, H_{HAZ} is the minimum hardness of the soft zone and H_{TMP} is the hardness of the BM furnace tempered samples. Furnace tempering of the DP steels was performed at $600^{o}C$ for 1 hour, which were then removed from the furnace and air cooled.

2.7 Fatigue and Fracture of Welds

2.7.1 Stress Concentrations

Stress concentrations, such as undercut, weld concavity and porosity to name a few, are known to reduce fatigue life and are characterized by the notch effect [8]. The (SCF) stress concentration factor, K_f, is the ratio of the peak stress at the notch tip to the nominal stress acting over the area:

$$K_f = \frac{\sigma_{Max}}{\sigma_{Nom}}$$

(4)

Where: K_f is the stress concentration factor, σ_{Max} the peak stress and σ_{Nom} the nominal stress.

The stress concentration may lead to a reduction in both the tensile strength and the fatigue life of the specimen [48]. Figure 11 shows the stress concentration of a specimen with two identical notches about one third of the thickness of the specimen. It can be observed that the peak stress occurs at the tip of the radii with a simulated SCF of 2.47. It should also be noted that the stress has risen adjacent to the notch tip as well.
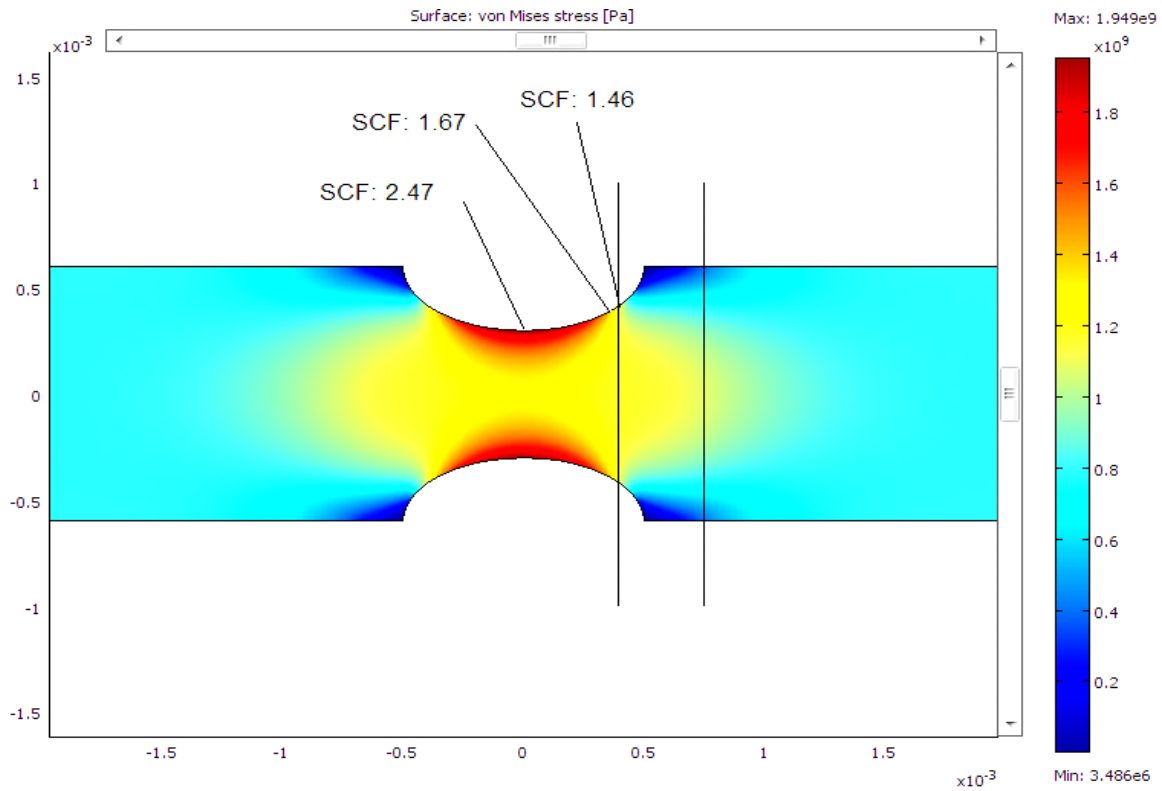
Figure 11: Simulated stress concentration factors for a specimen with symmetric notches one third the thickness of the specimen

2.7.2 Fatigue Mechanism

Fatigue failure occurs when stress amplitudes below the yield strength are repeatedly loaded on the weldment. This mechanism is known as fatigue and occurs in three stages (Figure 12); crack initiation, crack propagation and fracture [8].
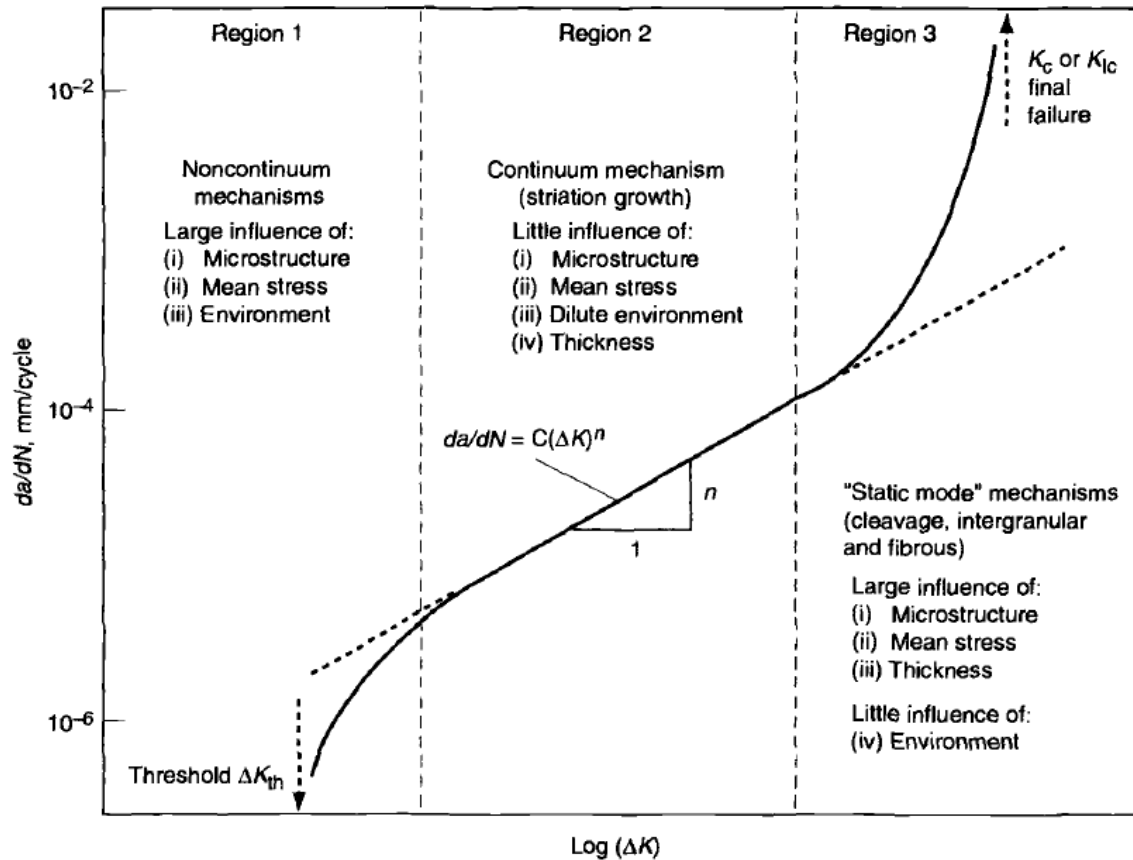
Figure 12: Regions of crack nucleation, growth and fracture [48]

Cracks initiate from surface discontinuities [8] when dislocations build up along the slip planes of the material near these surface discontinuities [48]. At low stress amplitudes crack nucleation is slow [48], and it is the ease of which cracks can be formed that determines the number of cycles to failure. On the other hand, when the applied stress amplitude is high, nucleation of cracks is fast and the fatigue life of the specimen is dominated by crack propagation [48]. Thus the presence of a macroscopic notch would increase the stress amplitude at surface discontinuities leading to easier crack nucleation.

Once a crack is formed it propagates through the material according to the Paris equation [48], where the change in crack length for a given number of cycles is related to the stress intensity range and material properties as:

$$\frac{da}{dN} = C(\Delta K)^n$$

(5)

Where, da is the change in crack length, dN the number of cycles, the stress intensity factor, and C and n are constants used to fit the data to the log da/dN vs. curves. Eventually the crack grows to a length at which the stress intensity at the notch tip reaches the stress intensity required for fracture at which point the specimen fails [48].

Crack propagation is faster for a brittle material as there is little elastic deformation within brittle material, leading to crack growth at the plastic zone of the notch tip [48], providing the stress concentration at the notch tip exceeds the material's strength.

2.7.3 Weld Concavity

Concavity is formed by metal ejection from the weld pool during welding [5]. There are reports on simulation of the keyhole dynamics in laser welding, which indicated that metal ejection from the weld pool depends on the welding parameters [11, 49]. However, metal ejection from the weld pool can also occur due to instability of the liquid phase especially when the vapour-liquid interface within the keyhole moves normal to the laser beam at high speeds [10]. Additional studies revealed that the depth and width of the keyhole fluctuated violently during welding, and the evaporation of the metal did not take place uniformly but locally from the front of the keyhole [6]; due to an imbalance of vapor pressure and surface tension metal ejection occurs as shown in Figure 13.
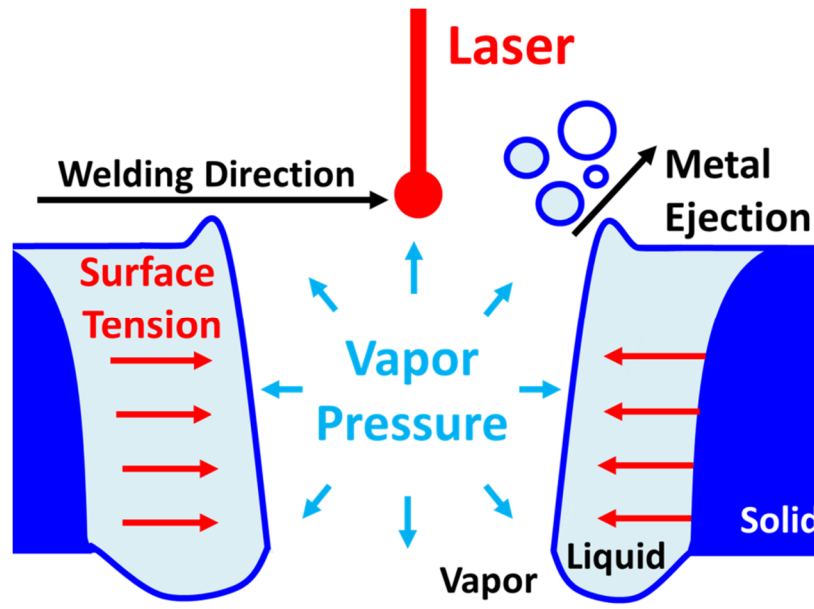
Figure 13: Metal ejection from weld pool in keyhole mode welding

An effective way to improve the weld quality is to reduce power and speed [7], but a reduction in speed is known to increase the severity of the HAZ softening [43]. Traditionally, laser welds exhibit a fatigue life comparable to the BM; however, recent studies have indicated that fatigue life of DP steel welded by fiber laser reduced by around 30% when compared to the BM [38] [39]. Also, the stress concentration at the concavity (acting like a notch) serves as the crack initiation site allowing the crack to propagate into the soft zone in the welds [38].

2.8   Summary

Several studies have been performed on the effects of HAZ softening in resistance spot welding, HPDL and Nd:YAG laser welding of DP steels. Several of these studies have reported on the degradation of tensile [41, 45-46, 50], formability [43, 51] and hardness properties [37, 52]

within the HAZ. Additionally researchers have also recently reported on the fatigue performance of HPDL welded DP joints [40] however little research has been reported the FLW of DP steels.

Xu *et. al.* recently examined laser welded DP steel made by both Fiber and Diode Laser [38, 39]. It was observed that both processes demonstrated HAZ softening, however the higher heat input welds of Diode Laser welds, exhibited a greater amount of softening, which then lead to poorer performance in tensile and fatigue testing. The large scatter in data of this data set was attributed to variations in weld concavity.

Chapter 3: Experimental Methods

3.1   Laser welding

An IPG Photonics YLS-6000 Ytterbium fiber laser system integrated with a Panasonic TA 1600 robot was implemented for welding. The laser medium was an ytterbium doped fiber, which provided a continuous wavelength output of 1071 nm. This fiber was then fed into an optic system with a collimating and focal length of 129 mm and 200 mm respectively. The power intensity of the laser beam delivered by the optics was scanned and the beam was observed (Figure 14) to possess a spot size of $0.28mm^2$, a divergence angle of 59.9 mrad and beam parameter of 5.8.

a)   b)
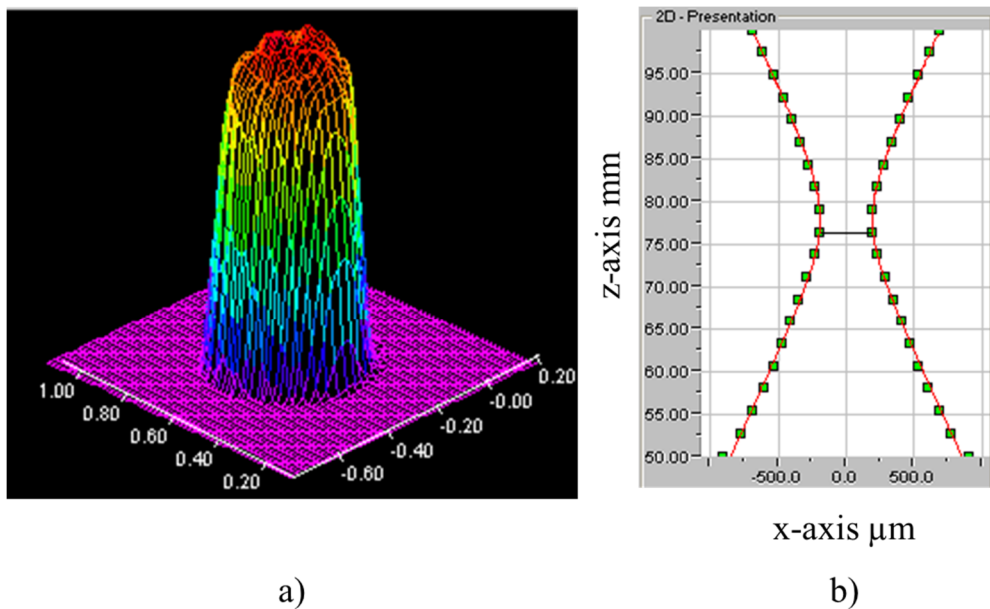
Figure 14: Laser beam profiles: (a) 3-D profile near spot size (b) 2-D profile showing beam divergence

Calibration of the equipment showed good correlation between the commanded laser power to the power delivered by the optics; the commanded power could be considered the same as the power delivered to the work piece, Figure 15.
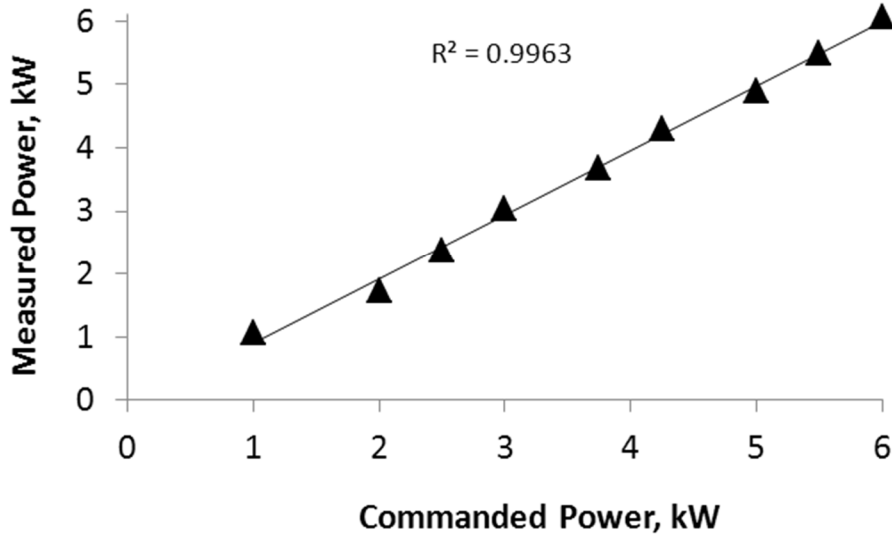
Figure 15: Correlation of commanded laser power and measured laser power

The robot enabled the system with 6 axes of freedom, yet for simplicity, linear welds were selected for evaluation. Process optimization trials revealed that a vertical head angle of 20° was necessary to prevent damage to the optics from weld spatter. Argon shielding gas could be provided to both the top and bottom side of the weld; a trial and error method was implemented to determine a low flow rate which would provide shielding such that severe oxidation was not present at any welding speed. Furthermore, an air knife was used to remove zinc vapors from the weld pool.

3.2   Materials

The steels investigated in this study were all hot dip galvanized sheets with a thickness of 1.2 mm. Three steels are investigated in this study, one HSLA steel and two DP980 steels, where the DP980 Rich steel was comprised by alloying additions of Cr, Mo, Mn and Si while the DP980 Lean steel was alloyed by Mn and Si additions; the chemical composition of all the steels are listed in Table 1.

Table 1: Chemical composition (wt-%) and mechanical properties of steels used

Steel	DP980 Rich	DP980 Lean	HSLA450
C	0.09	0.15	0.05
Mn	2.1	1.5	0.6
Si	0.3	0.3	0.1
Al	0.05	0.04	0.03
Cr	0.2	0.0	0.1
Mo	0.3	0.0	0.0
Ni	0.0	0.0	0.1
V	0.00	0.00	0.00
Ti	0.03	0.00	0.02
Nb	0.02	0.00	0.01
Fe	Bal.	Bal.	Bal.
T_M (^{o}C)	1513	1514	1527
T_{Ac1} (^{o}C)	713	717	721
YS (MPa)	618	697	415
UTS (MPa)	998	1083	461
Elongation (%)	14.0	12.2	30.7
Hardness (HV)	325	350	145
Vol. Martensite (%)	38.2	56.4	0.0
Vol. Bainite (%)	7.0	0.0	0.0
Vol. Ferrite (%)	Bal.	Bal.	Bal.

3.2.1 Joint Configuration

Steel sheets were cut to 200 mm × 100 mm pieces and then butt welded, with a single linear weld (SLW), to form a 200 mm × 200 mm blank (Figure 16). All the welds were made perpendicular to the rolling direction (RD) of the sheets (Figure 16). To attain the necessary joint fit up, the edges to be welded were machined flush; sheets were considered to align if there were no gaps larger than 0.05 mm, which was measured by a standard feeler gauge. Before welding, all the edges were de-burred while the surface of the sheets was washed with acetone. The steel sheets were clamped onto a jig fixed by machine clamps to avoid misalignment during welding.
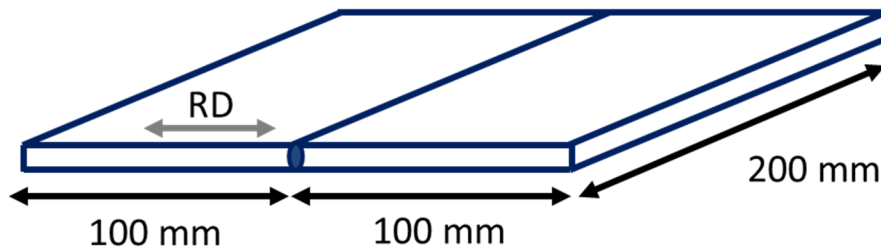
Figure 16: Schematic of joint configuration

3.2.2 Microstructure Examination

To examine the microstructure and weld profiles weld cross-sections were prepared by grinding using a series of SiC papers, followed by polishing with a 1µm diamond suspension. Then specimens were etched using a 2% Nital solution for about 4 to 6 seconds.

The weld profiles were observed in an Olympus BX51M optical microscope while higher magnification views of the microstructure were attained using a JEOL JSM 6460 scanning electron microscope.

Area fraction analysis was, using Image-J analysis software, to determine the volume fraction of phases present within the steel. The area fraction of the DP980 Rich steel is shown in Figure 17 where red is martensite, blue is ferrite and green is bainite.
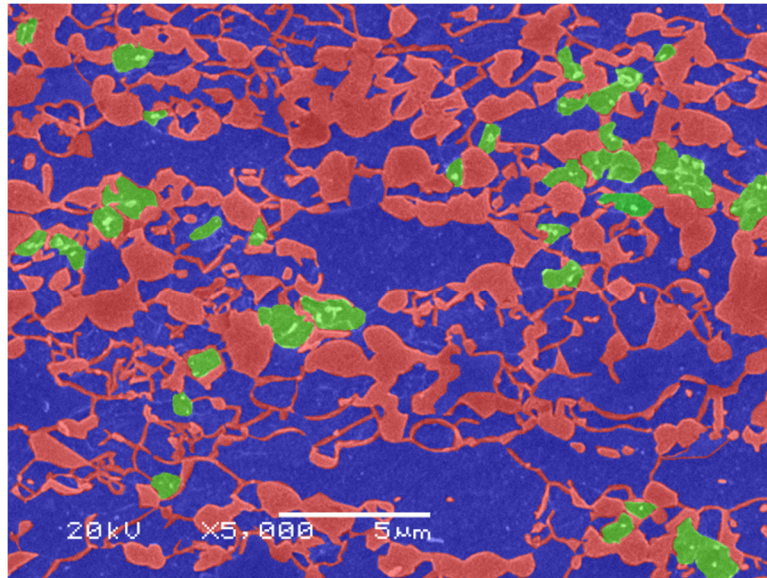
Figure 17: DP980 Rich microstructure shaded for area fraction analysis

Scanning electron microscopy (SEM) images demonstrating the microstructure of the base materials investigated in this study are shown in Figure 18, the volume fraction of different phases present within each steel are listed in Table 1. The HSLA steel was comprised of a fine grained ferrite with carbides dispersed throughout (Figure 18a), DP980 rich was comprised of ferrite (dark regions: Figure 18b) and martensite (bright regions: Figure 18b) as well as a small fraction of bainite (arrow: Figure 18b), while DP980 Lean was comprised of ferrite (dark regions: Figure 18c) and martensite (bright regions: Figure 18c).
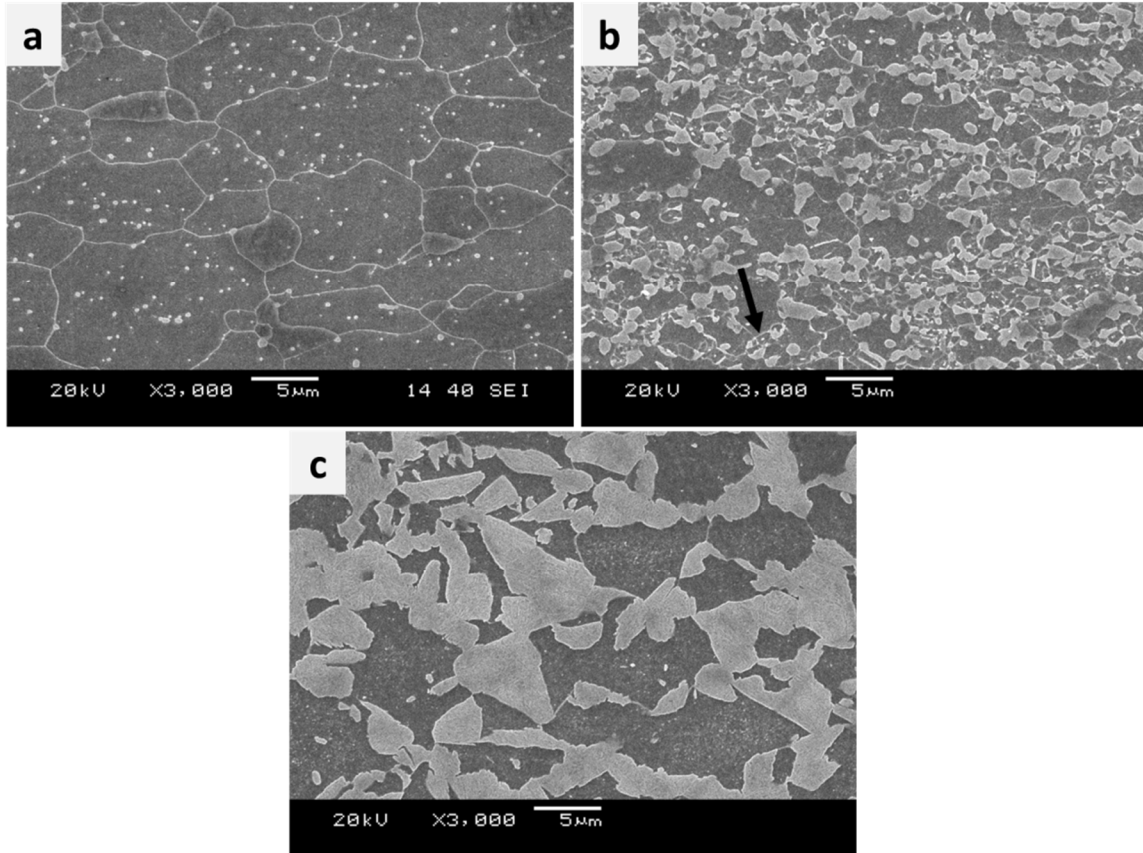
Figure 18: Base metal microstructure of the steels used: (a) HSLA (b) DP980 Rich (c) DP980 Lean

3.2.3 Concavity Measurement

Weld concavity is measured as the ratio of the reduction in area from the sheet thickness in the fusion zone to the initial sheet thickness, as outlined by GM4485M [53]; this measurement is illustrated in Figure 19 and further explained by Equation 6.
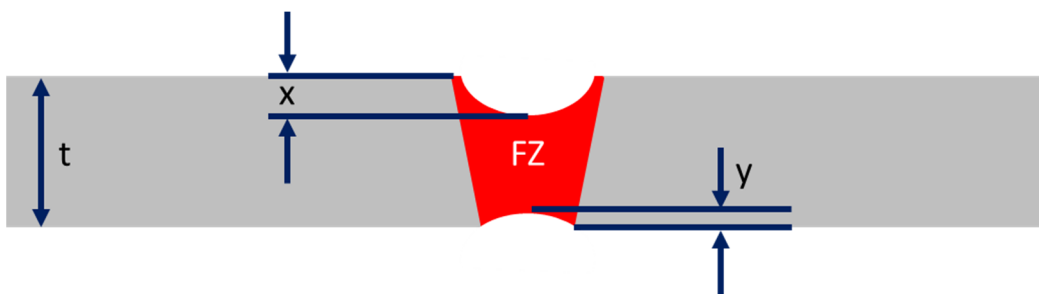
Figure 19: Schematic illustration of the concavity measurement

Thus:

$$Concavity = \frac{x + y}{t} * 100$$

<div align="right">(6)</div>

In thin sheets, the measurement is sensitive to error in the measurement, in order to make an effective comparison, concavity values were binned into ranges of about 5%. In other words concavity measured over the ranges of 0%, 11-13%, 14-16%, 23-28%, and 33-38% are reported as 0%, 10%, 15%, 25%, and 35%, respectively.

3.3   Mechanical Testing

3.3.1   Hardness Profiling

Microhardness profiles were obtained across the etched specimens of the welds in a Clemex-JS 2000 automated hardness tester using a 200 gram load and 15 s dwell time. The hardness indentations were spaced at least three diameters from one another to avoid interference from the strain fields of the adjacent indents. A second hardness profile with high resolution was developed in order to capture hardness of the narrow HAZ created by FLW, a staggered pattern was used as shown in Figure 20 the hardness profile was staggered about the weld centerline in the x-axis and positioned 350 µm form the top side of the weld.
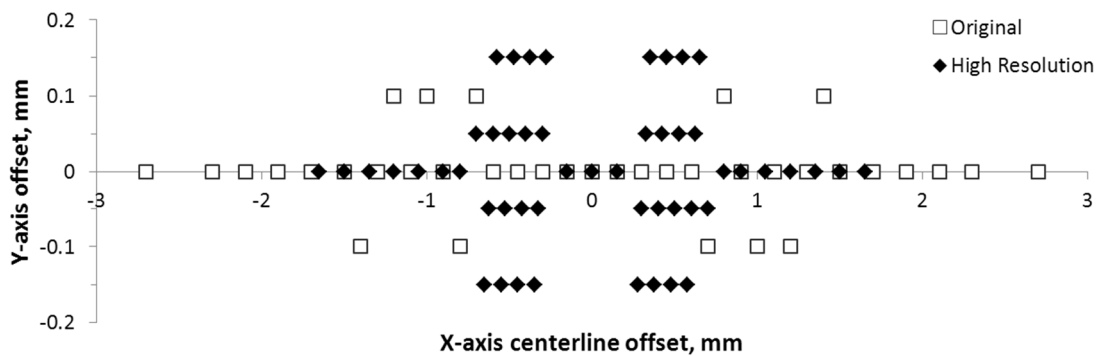
Figure 20: Hardness profile indentation points relevant to weld centerline

36

3.3.2 Tensile Testing

Transverse tensile specimens, with the welds centered at the gauge length (Figure 21), were machined from the welds as per ASTM: E8 standards. The first and last inch of the blank were discarded to remove any possible effects of the weld start and crater. The tensile tests were performed using a crosshead speed of 2.54 mm/min. For the welds with concavity, only the peak loads obtained from the tensile tests were analyzed to minimize the error that may arise due to changes in the cross-sectional area in the gauge length because of the concavity.

Figure 21: Position of welds on the tensile specimens

3.3.3 Fatigue Testing

ASTM: E8 specimens (Figure 21) were also used for cyclic fatigue testing. A fully computerized Instron 8801 servo hydraulic testing system with a stress ratio of R=0.1 applied in a sinusoidal wave at 50Hz was used to evaluate fatigue performance according to ASTM:E466 test standards. When a specimen was capable of sustaining 10^7 cycles without failure it was considered to have reached its fatigue limit; the stress amplitude at which a specimen endured infinite life. The fracture surfaces of the tensile and fatigue tested specimens were observed using a JEOL JSM 6460 scanning electron microscope.

3.3.4 Formability Testing

Limiting dome height (LDH) testing was performed using a 101.6 mm (4 inch) hemispherical punch on a hydraulic press. Laser welded blanks, made with SLW, were cut to 200 mm x 200 mm sheets and were then orientated on the lower die so that the weld bottom was in contact with

the hemispherical dome, with the weld centered about the middle of the die opening, as shown in Figure 22. Clamping pressure was applied between the upper and lower die to prevent the specimen from slipping between the dies during forming. Prior to forming the steel sheets were lubricated lightly using a mill oil. The test was stopped upon the formation of a visible fracture. The dome height was then measured using a height gauge; the gauge's accuracy was verified to be within 0.1 mm using standard height blocks.
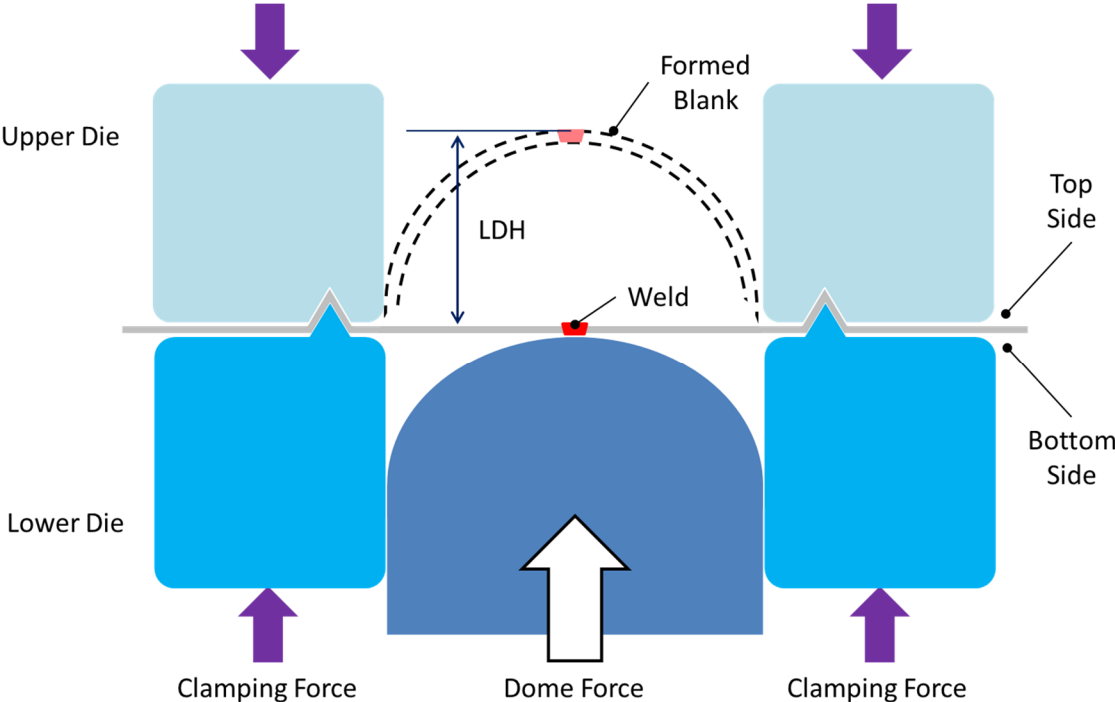
Figure 22: Schematic of limiting dome height test

Chapter 4: Effects of Weld concavity on Mechanical Properties of Fiber Laser Welds

4.1   Weld concavity

The speed and power levels examined in this study are shown in Figure 23 and example profiles of the resultant weld geometries are shown in Figure 24.
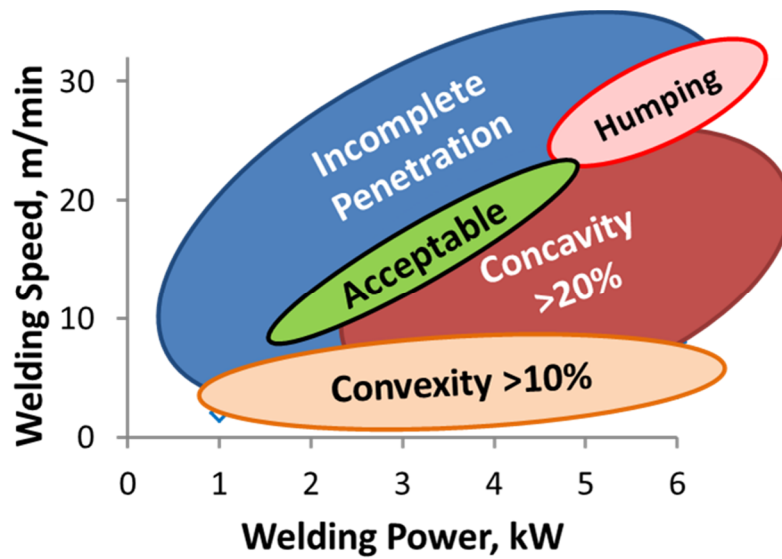
Figure 23: Process envelop of 1.2mm thick steel sheet made by FLW
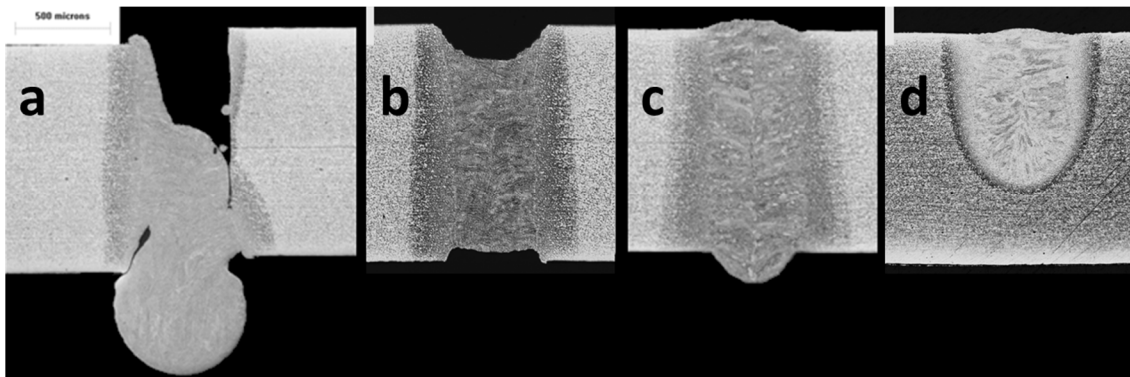
Figure 24: Weld profiles of typical geometries observed a) humping b) concavity c) convexity d) incomplete penetration

Using 6 kW full penetration welds could be made at 30 m/min (Figure 23); however, at welding speeds higher than 22 m/min a cyclic formation of severe concavity at the top of the weld and severe convexity on the bottom of the weld occurred (Figure 24a), creating a discontinuous weld profile with large reductions in area from the BM; otherwise known as weld humping. Welds with humping were very weak, and could be broken by hand. Concavity occurred when weld cross sections experienced a reduction in area which is well wetted to the surrounding material (Figure 24b). Convexity (Figure 24c), being constant without cyclic formation, occurred when a continuous well wetted convex dome formed on either the top or bottom side of the weld along the length of the weldment. Incomplete penetration (Figure 24d) occurred when the heat input was too low to melt the bulk material. Welds were considered acceptable (Figure 23) when they form less than 20% concavity, have convexity below 10%, and were free from other defects, as per current industry standard: GM4485M [53]. Acceptable welds were made by increasing welding speed, at constant power, so that the welds just fully penetrated the sheet thickness. Accordingly, the welding speed for making acceptable welds was observed to increase with increasing power (Figure 23). For example, using 2 kW power acceptable welds could be formed at a lower speed of 10 m/min whereas increasing the power to 4 kW required a higher speed (20.5 m/min). However, increasing power beyond 4 kW and decreasing it below 2 kW could not form acceptable welds. So, it was observed that to make acceptable welds in 1.2 mm thick sheets a power range of 2-4 kW with speed of 10-20.5 m/min is required. Fully penetrating weld profiles possessing the least amount of concavity at each power level are shown in Figure 25. Welds made at 1 kW were unacceptable because it contained porosity (Figure 25a). It was also observed that the concavity increased with power (Figure 25b-f).
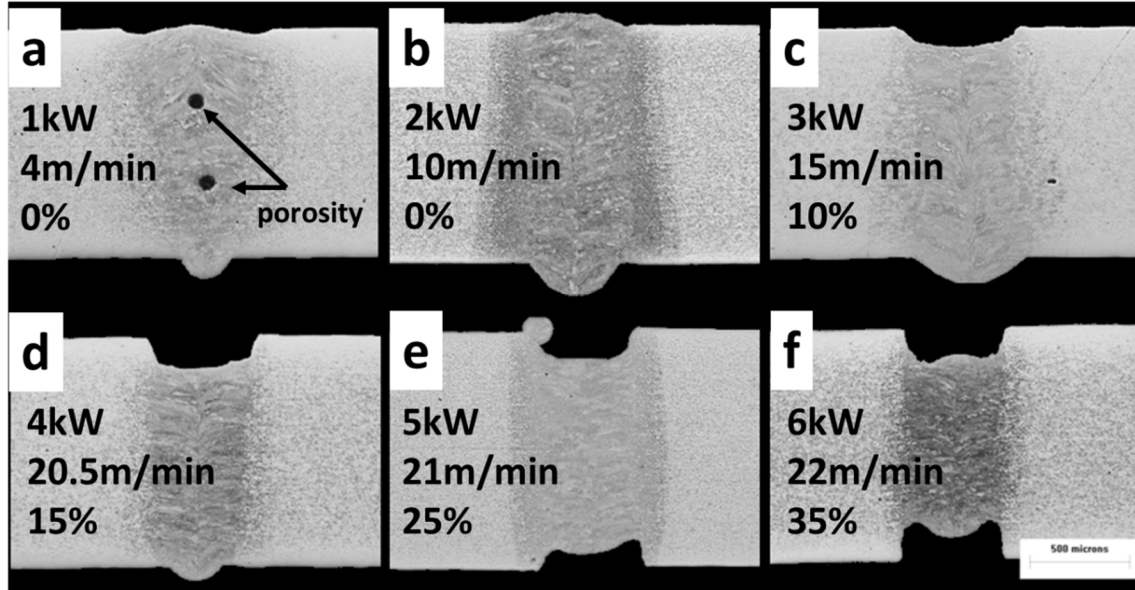
Figure 25: Best weld geometry attained studied power levels

The formation of concavity due to keyhole instability may be explained by the ejection of metal from the weld pool, which has been reported earlier [5, 7, 10-11, 49]. Furthermore the amount of metal loss was measured by using a mass balance, as outlined in Appendix A, and it was determined that the weld concavity was a result of metal ejection from the weld pool. In keyhole mode welding, evaporation of the molten metal takes place leading to an increase in vapor pressure, which pushes the vapor-liquid interface ahead of the laser beam [10]. High vapor pressure can result in higher melt velocities causing ejection of the weld metal from the front of the weld pool. Therefore, the complex liquid motion within the weld pool determines the resultant weld geometry [10]. Furthermore, a recent simulation study [11] reported that the driving force for moving the vapor-liquid interface is the vapor pressure of the keyhole. The vapor pressure depends on the available heat in the keyhole and for a constant spot size an increase in the beam power increases the vapor pressure. Thus, an increase in laser power, at any given speed, would result in a greater amount of metal ejection from the weld pool [11], which

41

was also observed in the present study (Figure 25c-f). At any given power, welding speed controls the size of the vapor column; in other words the ability to evaporate the liquid phase and maintain a constant keyhole size is determined by the welding speed [10]. Therefore, too high of a welding speed would cause the keyhole to become unstable [7, 10-11] as was observed by the erratic humping (Figure 24a) formed above 22 m/min (Figure 23). Alternatively, the welding speed determines penetration depth [5] as was observed for lower power (1-4 kW) where higher speeds yielded incomplete penetration (Figure 23).

4.2 Microhardness and tensile properties

Figure 26 shows the hardness profiles across the welds of DP980 Lean and HSLA450 steel made with 4 kW power and 20.5 m/min speed; where the upper and lower 95% confidence intervals indicate the expected hardness range based on statistical probability. In the fusion zone (FZ) DP980 steel attained higher hardness (~480 HV) than HSLA steel (~350 HV) (Figure 26).
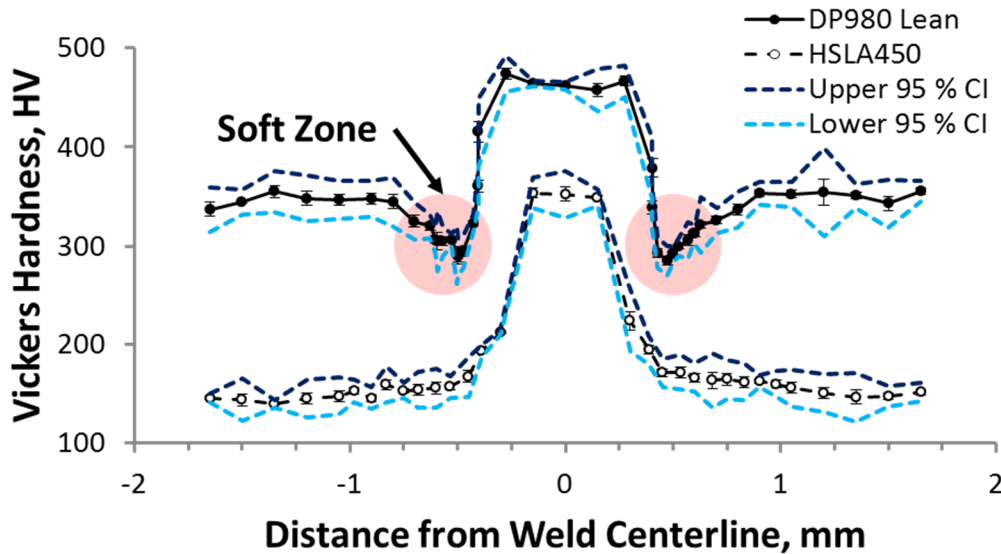
Figure 26: Microhardness profile of DP980 Lean compared to HSLA450 steel, with welds made at 20.5m/min and 4 kW

HAZ softening was detected in the DP steel, as indicated on the profile (Figure 26) with a minimum hardness of about 300 HV; exact values for examined speed-power combinations are listed in Table 2. HAZ softening is related to tempering of the martensite phases present in the BM (Figure 18) because the temperature experienced in this region during welding approaches the Ac_1 temperature of the steel [22]. HAZ softening was not observed in the HSLA steel because martensite was absent in its BM (Figure 18).

Table 2: Tensile and soft zone properties of welds made with varied amounts of concavity

Steel	Speed (m/min)	Power (kW)	Concavity (%)	Soft Zone Hardness (HV)	Failure Location	Peak load (kN)
DP980 Lean	22	6	35	306	HAZ	14.1
DP980 Lean	21	5	25	307	HAZ	14.9
DP980 Lean	20.5	4	15	302	HAZ	15.2
DP980 Lean	15	3	10	295	HAZ	15.2
DP980 Lean	10	2	0	293	HAZ	15.2
HSLA450	22	6	35	…	BM	6.7
HSLA450	21	5	25	…	BM	6.5
HSLA450	20.5	4	15	…	BM	6.6
HSLA450	15	3	10	…	BM	6.5
HSLA450	10	2	0	…	BM	6.6

Tensile results (Figure 27) indicated that increasing concavity decreased the peak load in the DP980 welds whereas HSLA welds were not affected by concavity. Data analysis performed, assuming a normally distributed sample and using t-tests, suggested that for DP980 there was no significant change in the peak load within 0% to 15% concavity (Table 2). Thus, welds with 15% concavity were considered acceptable with respect to tensile strength and industry standards [53].
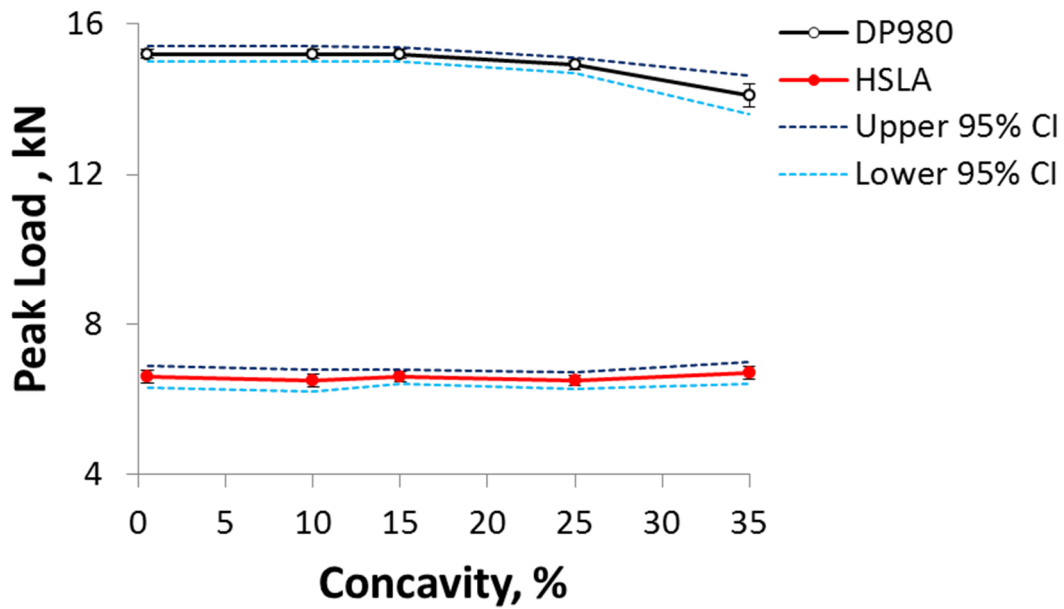
Figure 27: Relation of weld concavity to peak load carrying capacity for DP980 Lean and HSLA450

Alternatively, when the amount of concavity increased to 25% the peak load decreased (Figure 27) and continued to decrease with further increase in concavity (35%). A 1.1 kN drop in the peak load was observed in the DP980 steel when concavity was increased from 15% to 35% (Figure 27 and Table 2). The DP980 welds failed in the soft zone (Table 2) where strain localization occurred leading to premature failure [34, 43, 46], which was confirmed by the fractured surface showing typical ductile dimple morphology (Figure 28). The decrease in peak load for welds with 25% and 35 % concavity was attributed to the increased amount of concavity but not to the softening since the change in softening was reduced (Table 2); it was expected that reduced softening would increase the tensile strength as observed in previous studies [34, 37]. Although all welds failed in the soft zone, it is believed that the higher stress concentration, caused by larger concavity (acting like a notch), reduced the peak load leading to premature failure in the soft zone.
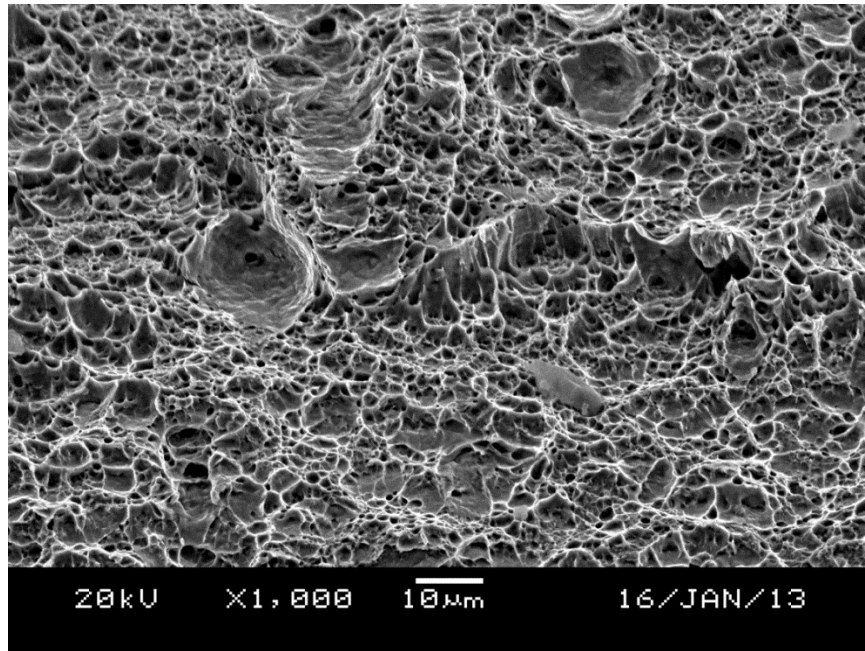
Figure 28: Ductile fracture surface of welded DP980 Lean

HSLA steel always fractured in the BM (Table 2) and increasing concavity was not observed to influence the peak load (Figure 27). The HSLA steel exhibited a resistance to the concavity because, unlike the DP980 steel, the HAZ in HSLA steel was stronger compared to the BM (Figure 26) and therefore deformation was concentrated in the weaker BM. The relative strength of the HSLA steel is further discussed in Appendix B. Based on the reduced concavity, reduced softening and higher peak load, 4 kW power with a welding speed of 20.5 m/min were considered the best welding parameters, resulting in only 15% concavity (Figure 25).

4.3   Fatigue resistance

S-N curves of the DP980 and HSLA welds are shown in Figure 29 and Figure 30, respectively. At a higher stress amplitude (450 MPa for the DP980 steel and 200 MPa for the HSLA steel), all welds exhibited similar fatigue resistance as their respective BM as observed in previous studies [38, 39].

45
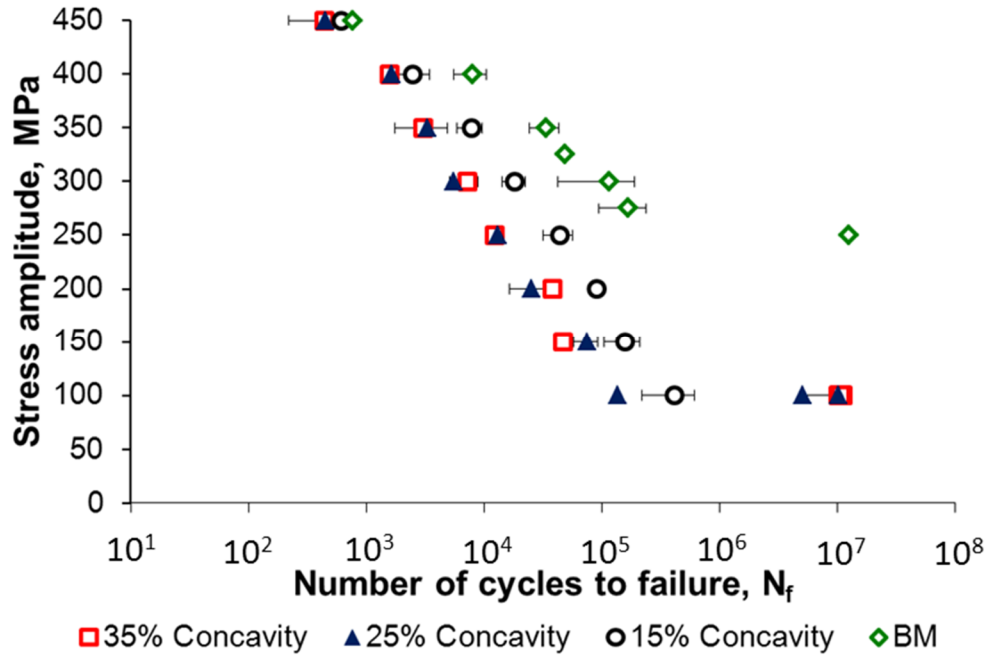
Figure 29: S-N curve of welded DP980 Lean with varied concavity compared to the BM
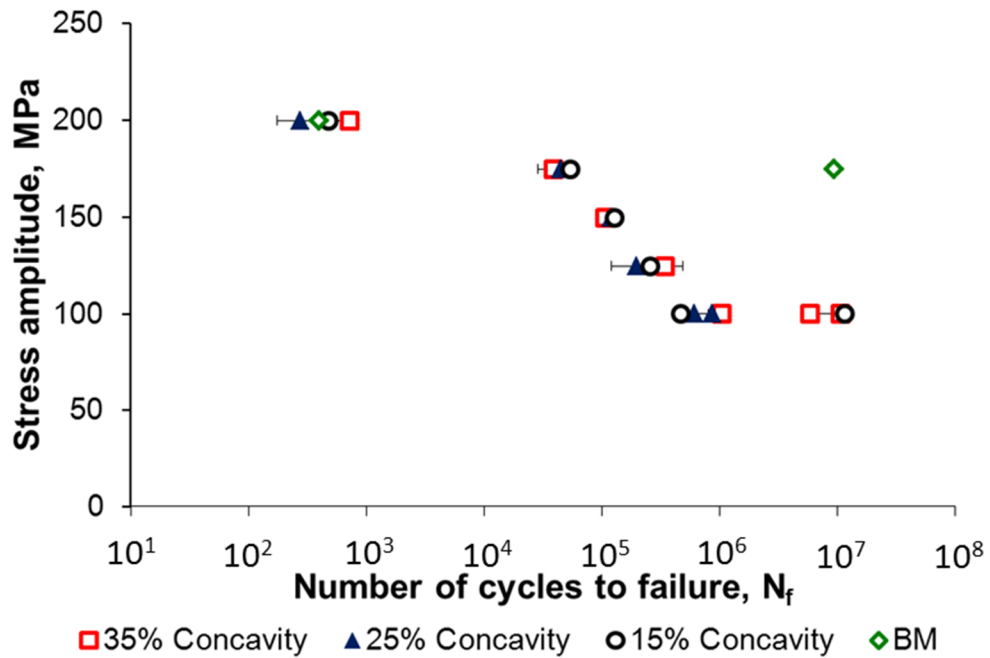
Figure 30: S-N curve of welded HSLA450 with varied concavity compared to the BM

At moderate stress amplitudes (350 MPa to 150 MPa for the DP980 steel and 175 MPa to 100 MPa for the HSLA steel), a significant reduction in the fatigue life of all the welds was observed when compared to the BM (Figure 29 and Figure 30). DP980 steel welds having higher concavity (25 and 35%) demonstrated an even further reduction in fatigue resistance at moderate stress amplitudes (Figure 29) compared to welds with lower concavity (15%); while HSLA welds with different amounts of concavity showed similar fatigue resistance. This difference in concavity (notch) sensitivity could be attributed the difference in weld hardness in both steels. The lower hardness (Figure 26), and thus more ductile HSLA welds, would yield lower notch sensitivity than the harder DP980 welds [48]. However, the reductions in ductility and changes in the weld geometry, as will be shown later, still decreased the fatigue resistance of the HSLA welds compared to the BM (Figure 30).

Welding reduced the fatigue limit of both the steels; DP980 welds showed a 63% reduction while HSLA steel showed a 43% reduction when compared to their respective BM. For DP980 welds, lower concavity (15%) welds did not yield infinite life unlike the higher concavity (25% and 35%) welds (Figure 29); possible reasons are discussed later in this section.

The fatigue fracture surface of the DP980 welds showed that the cracks initiated at the surface defects in the FZ on the concavity and then propagated throughout the FZ (Figure 31a). The crack initiation was determined by the radiating structures from the concavity (Figure 31a), which was seen to start either at the bottom side of the concavity (Figure 31b) where weld spatters were present (Figure 31c) or at the topside of the concavity (Figure 31d) where ripples in the weld bead created surface discontinuities (Figure 31e). The crack then propagated through the highly hardened (Figure 26), and thus more notch sensitive FZ as confirmed by the cleavage morphology (Figure 31f). Figure 32a-b shows a transition from brittle cleavage like fracture

(Figure 32c) to a mixture of brittle cleavage and ductile dimple morphology (Figure 32d). The final fracture surface demonstrated a typical dimple structure (Figure 32e), which confirmed that final fracture in the DP980 welds occurred in the soft zone. Fracture propagation into the soft zone was also observed by the slight necking (bright regions), at the outer edges of the fractured specimens (Figure 33a-c).

For HSLA steel welds, fatigue crack initiation began at surface discontinuities due to ripples formed in the areas of high concavity (Figure 34a-b), which then propagated through the harder FZ until stress was concentrated at the edges of the specimen. In the failed specimens necking was observed (Figure 33d-f), which resulted in ductile failure as indicated by typical dimple morphology (Figure 34c). For HSLA welds, the observed deformation was more uniform indicating that the final fracture occurred in the BM, as confirmed by the large amount necking at the outer edges of the failed specimens (Figure 33d-f), with fracture propagating through the harder FZ and HAZ.
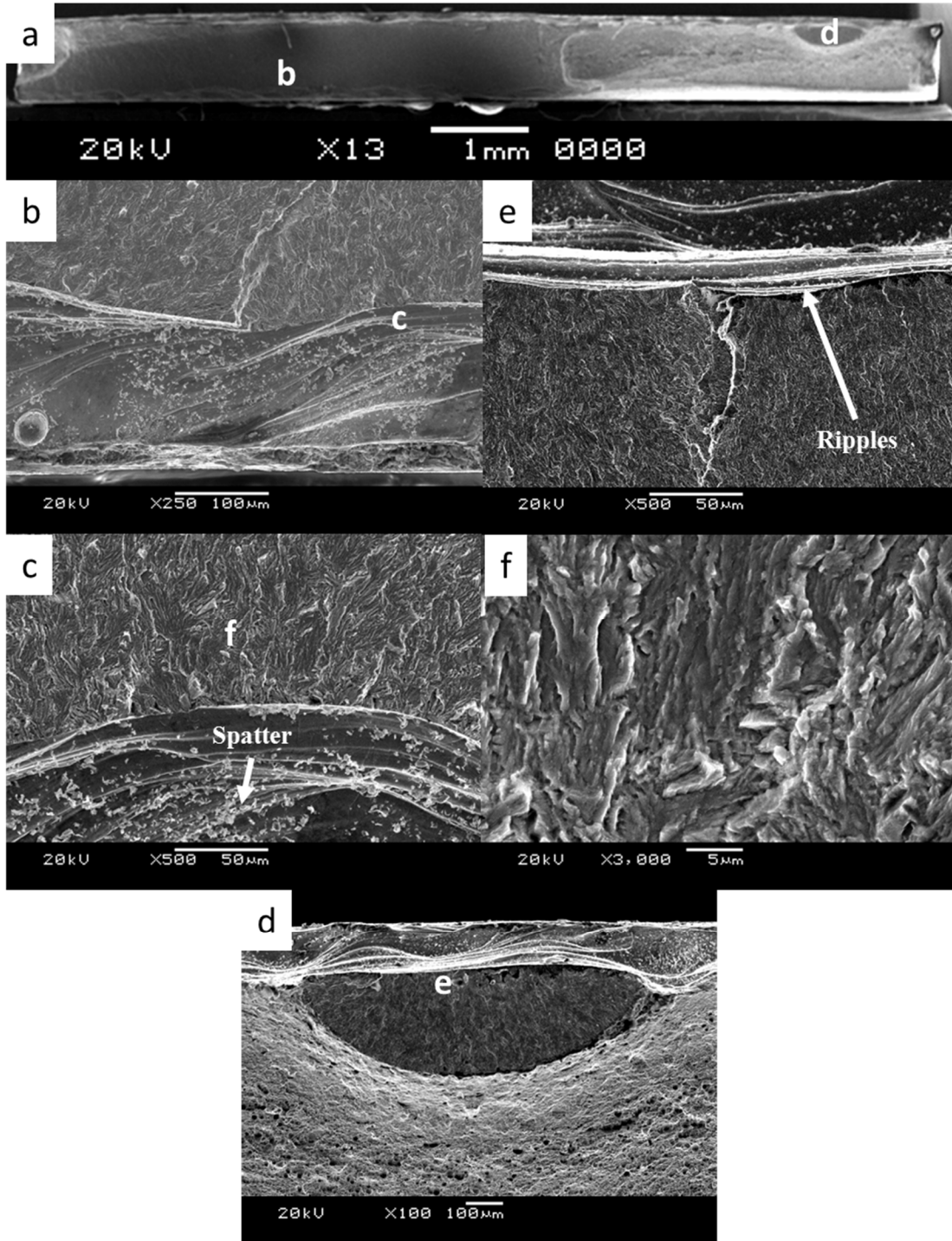
Figure 31: Fracture surfaces DP980 lean steel at low stress amplitudes (150MPa)
a) transverse fracture surface b) crack propagation leading to bottom side concavity (c) crack initiation at weld spatter (d) crack propagation leading to top side concavity (e) crack intiation at ripples of weld bead (f) brittle cleavage at initiation
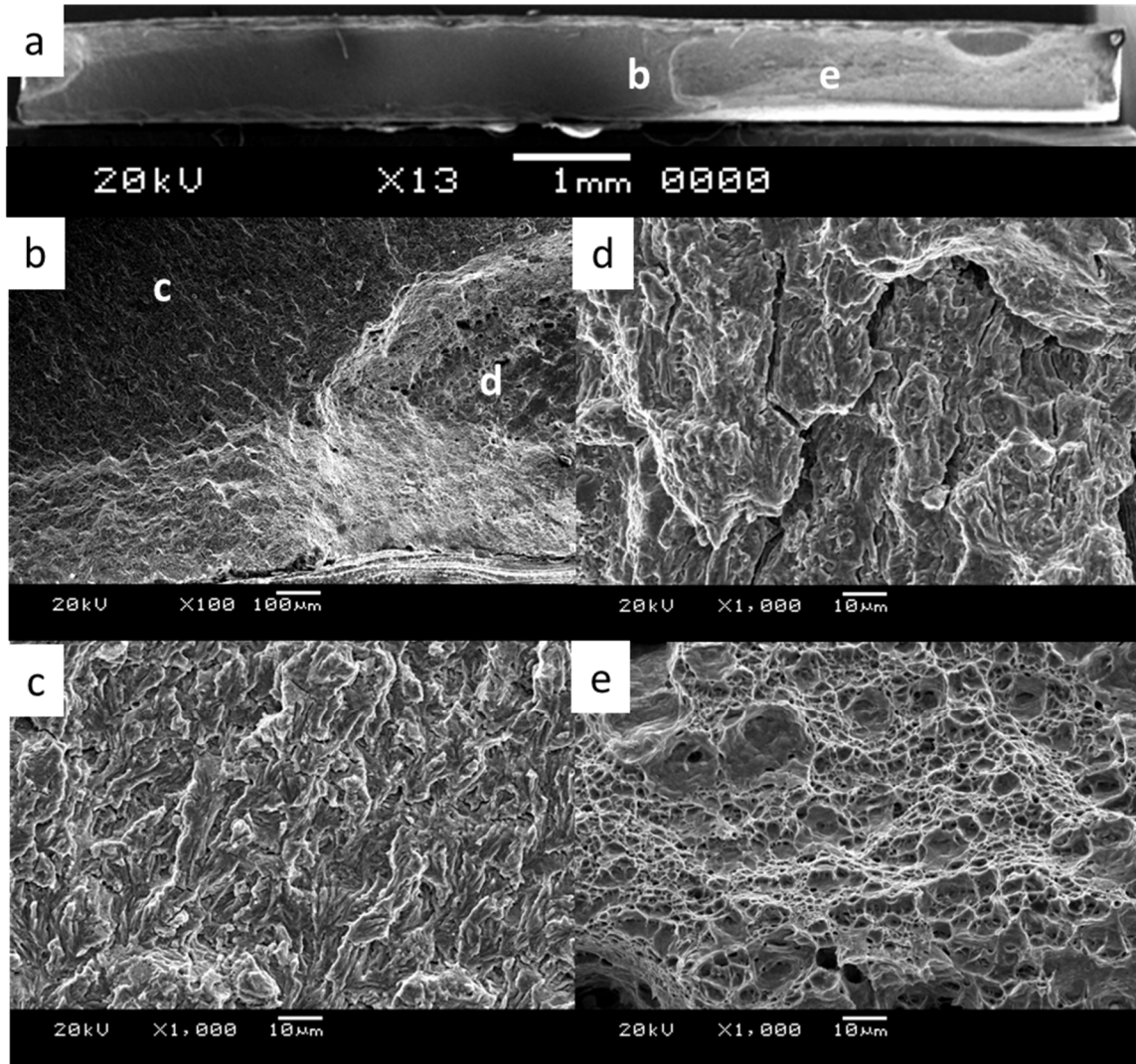
Figure 32: DP980 Final fracture surfaces at low stress amplitude (150MPa)
(a) fracture profile, same as Figure 13a (b) transition from brittle to ductile fracture (c) brittle propagation in FZ (d) cup-cone and brittle cleavage mix (e) ductile cup-cone fracture surface

Surface discontinuities in the DP980 welds were observed to have significant effect on the fatigue life at the low stress amplitudes (Figure 29), which is well supported by literature [48]. It should be recalled that the welds with 15% concavity were made at a speed so that the laser just fully penetrated the sheet thickness (Figure 25d), which formed weld spatters on the bottom side of the weld (Figure 31c). The weld spatters acted as crack initiation sites and reduced the fatigue life of the DP980 welds with 15% concavity, compared to the welds with higher amounts of

50

concavity which attained infinite life (Figure 29). The ease of crack initiation at the spatters, compared to the ripples on the weld bead, decreased the fatigue life of welds with spatter at low stress amplitude. Thus, it was concluded that concavity had a significant effect on the fatigue resistance of DP980 steel welds at moderate stress amplitudes (350 to 150 MPa), while the surface conditions dominated the fatigue life at lower stress amplitude.
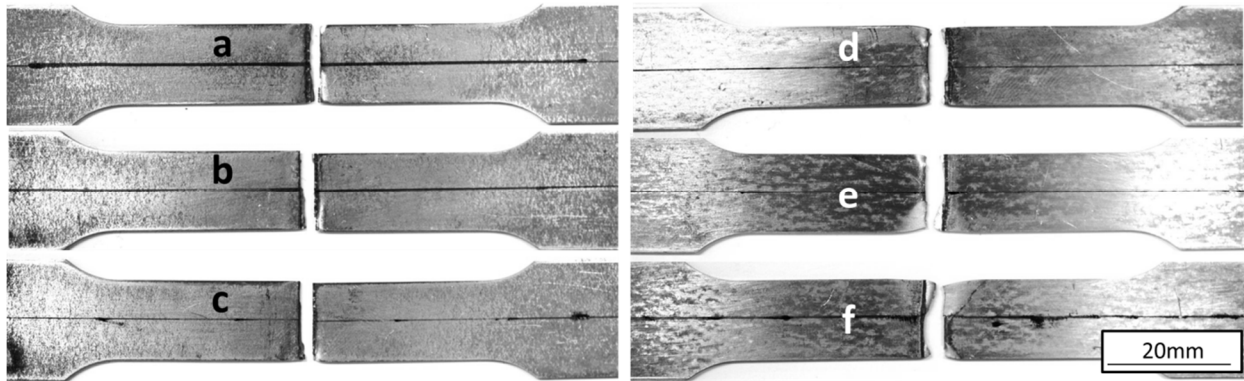
Figure 33: Macro image of fractured fatigue specimens
With DP980 Lean with concavity of a) 15% b) 25% c) 35% and HSLA with d) 15% e) 25% f) 35%
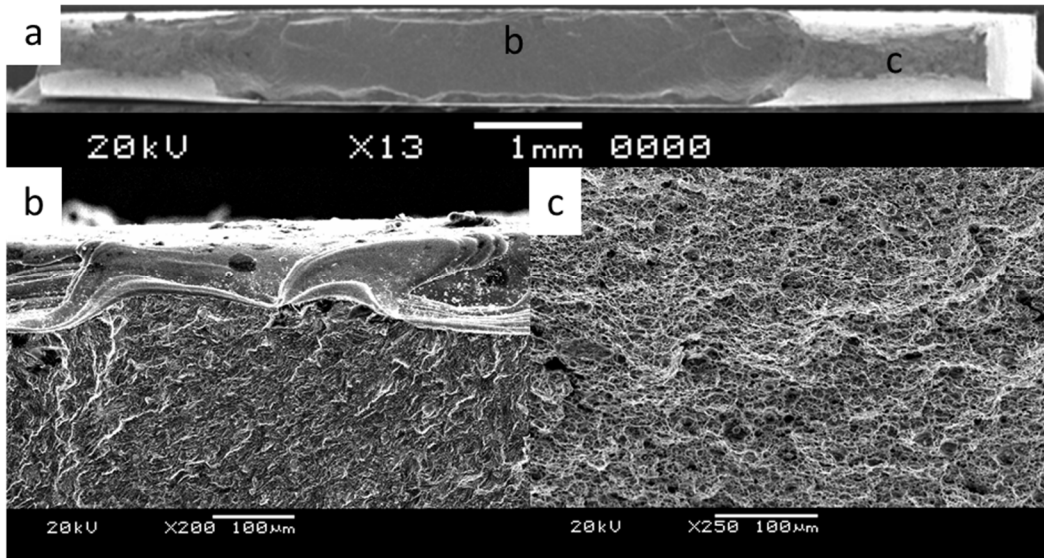
Figure 34: HSLA fracture profile for low stress amplitudes (100MPa).
(a) Fracture surface (b) crack initiation at ripples of weld bead (c) cup-cone fracture pattern of final fracture

Chapter 5: Mechanical properties and microstructure formation in Fiber Laser Welded Dual Phase and HSLA steels

5.1 Hardness

The hardness profiles of the DP980 Lean, DP980 Rich and HSLA450 FLW are illustrated in Figure 35, Figure 36 and Figure 37 respectively; where the upper and lower 95% confidence intervals identify the upper and lower bounds of the hardness values based upon the statistical probability of the observed data set. The metallurgical changes caused by FLW resulted in a large variation in the hardness across the weldments. For all steels the FZ greatly increased in hardness compared to the BM. The width of the fusion zone in all steels was found to be in the range of 450 to 550 µm. Welded DP980 Lean possessed a FZ with an average hardness of 468 HV, while the welded DP980 Rich steel yielded an average hardness of 420 HV and the welded HSLA steel yielded 353 HV (Table 3); this difference in hardness is attributed to the difference in carbon content of the steels, see Table 1.
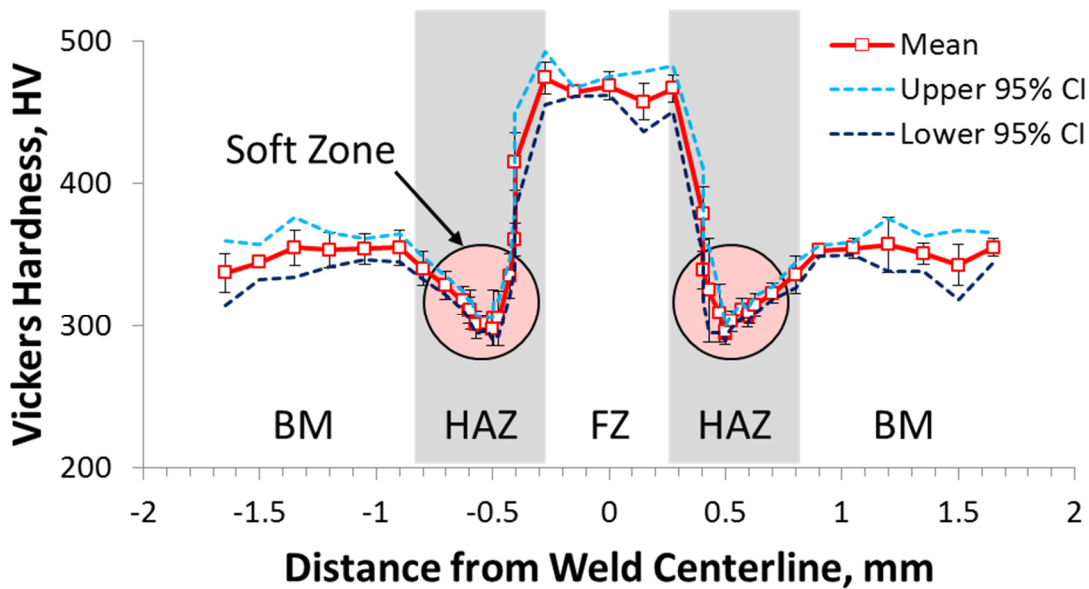
Figure 35: Hardness profile of welded DP980 Lean steel

52
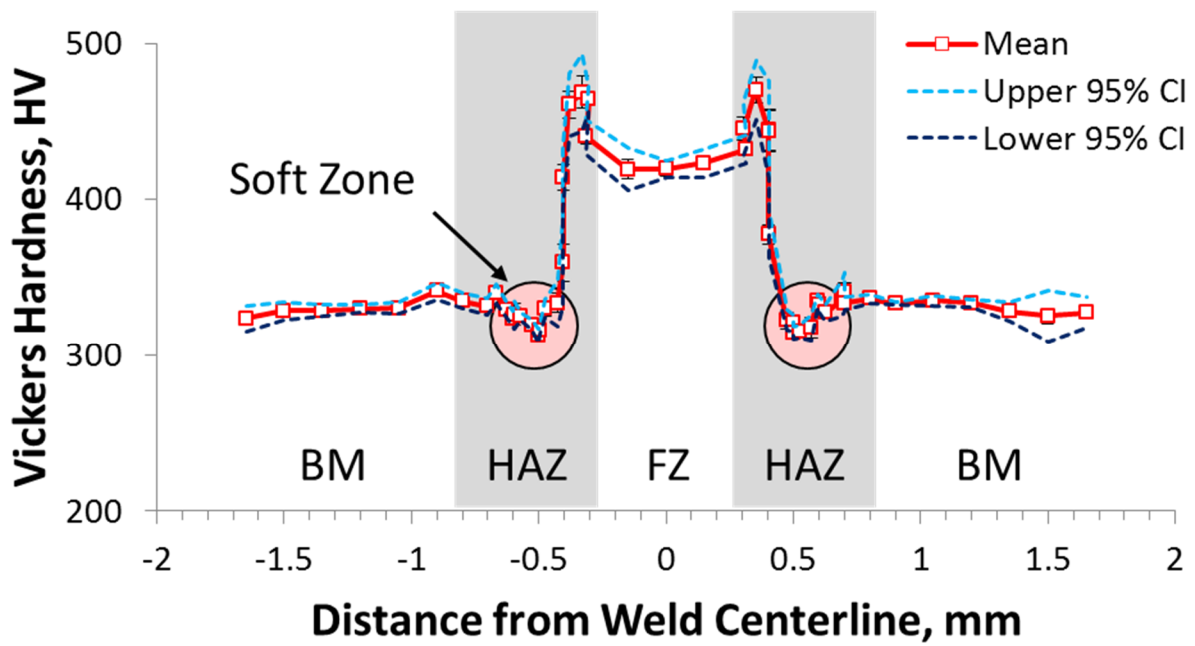
Figure 36: Hardness profile of welded DP980 Rich steel
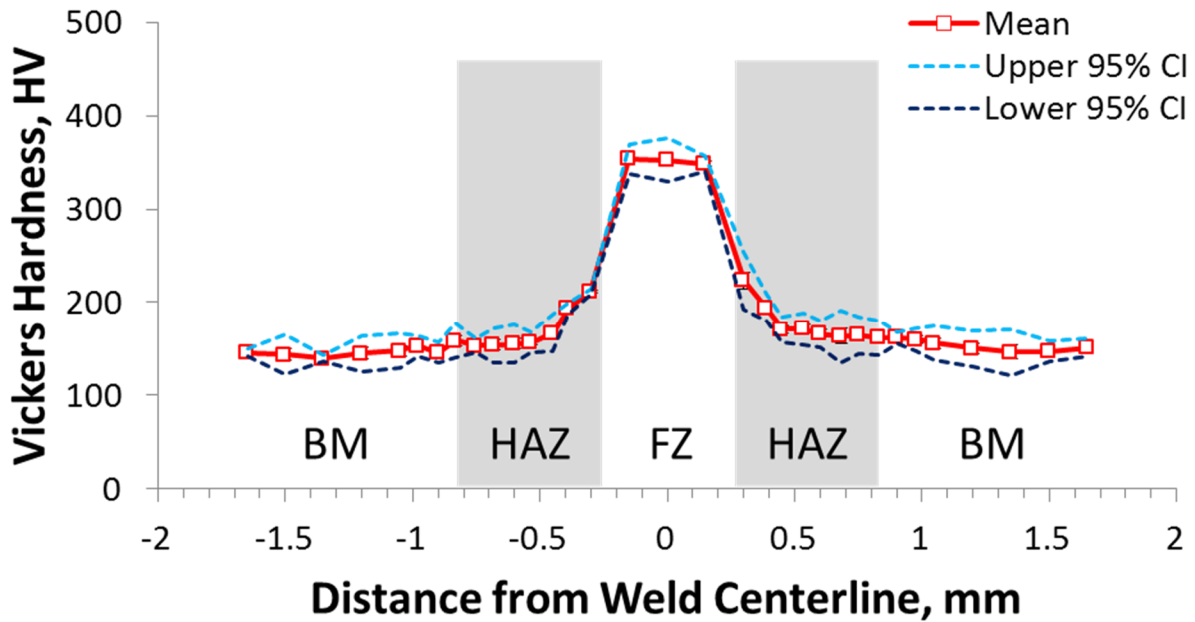
Figure 37: Hardness profile of welded HSLA450 steel

Yurioka *et. al.* [54] showed that the hardness of martensite could be predicted by the carbon content of the steel using Equation 7:

$$H_M = 884C(1 - 0.3C^2) + 294$$

<div align="right">(7)</div>

From Equation 7 it is clear that higher bulk carbon content leads to a harder martensite phase, as was also observed in the literature [54]. The predicted and measured values of the maximum hardness are listed in Table 3, interestingly the measured values exceed those of the predicted martensite hardness. Yurioka *et al.* observed that a higher cooling rate, such as those achieved by arc strike (where the arc welding torch was touched and the quickly removed), resulted in higher hardness values than predicted; an increase in cooling rate lead to an increase in the martensite hardness. Laser welding possess a much higher cooling rate than arc welding due to its higher speed [7-8, 10]. This high cooling rate leads to finer grain size in the FZ, which would cause an increase in hardness [28, 30-31]. Therefore, the higher FZ hardness in the DP980 Lean was concluded to be a result of the higher carbon content of the steel compared to the DP980 Rich and HSLA450 steels (Table 1)

Table 3: Predicted and measured hardness values

Steel	DP980 Rich	DP980 Lean	HSLA450
Predicted Hardness H_M (HV)	373	426	338
Measured Hardness (HV)	420	468	353
Carbon Content (wt-%)	0.09	0.15	0.05

The hardness profiles of all the steels; DP980 Lean (Figure 35), DP980 Rich (Figure 36) and HSLA (Figure 37), showed a steep gradient in which the hardness of the material rapidly

increased as the FZ was approached. Interestingly, the hardness was observed to drop significantly below the BM hardness in both DP980 steels at the subcritical HAZ (marked as soft zone; Figure 35 and Figure 36) which is well known as HAZ softening [34, 37, 47, 55]. The width of the soft zone for DP980 Lean and DP980 Rich was measured to be about 400 µm and 100 µm, respectively. The soft zone width was also found to decrease with increases in the welding speed (Table 4). Furthermore the reduction in the BM hardness i.e. severity of softening was also observed to decrease with increasing welding speed (Table 4); softening is defined as:

$$Softening = H_{BM} - H_{HAZ}$$

(8)

Where H_{BM} is the BM hardness and H_{HAZ} is the minimum hardness observed in the HAZ. Softening was not observed in the HSLA450 welds (Figure 37) because the BM did not contain martensite (Figure 4).

The high speed achieved in the FLW led to the very narrow HAZ compared to those obtained in Nd:YAG and diode laser welding [43]. A comparison of the present results with our previous works on diode and Nd:YAG laser welding [34, 56] is given in Table 5. It should be noted, that although the welding parameters match those of the weld concavity study, a higher resolution weld profile was used (Figure 20) which better captured the minimum hardness of the narrow HAZ made by FLW.

Table 4: Soft zone properties of welded DP980 Rich and Lean steels

Steel	Power (kW)	Speed(m/min)	Softening (HV)	Soft Zone Width (µm)
DP980 Lean	4	20.5	60	400
DP980 Lean	2	10	66	650
DP980 Rich	4	20.5	15	100
DP980 Rich	2	10	20	200

Table 5: Comparison of FZ and HAZ of DP980 Lean steel obtained in the present study using FLW with the earlier reports on diode and Nd:YAG laser welding [34] , [56]

Laser	Welding Speed (m/min)	Min. Soft Zone Hardness (HV)	Soft Zone Width (mm)	FZ Width (mm)
Fiber	20.5	290	0.4	0.45
Nd:YAG	6.0	260	0.5	0.5
Diode	1.2	233	2.5	3.2

To compare the tempering kinetics of welds made with different laser types having varied laser beam spot sizes, power intensities and beam characteristics, the time constant (τ) was used. The time constant, given in Equation 2, represents the time the material was heated at the Ac_1 temperature. To compare steels with a difference in martensite content the HAZ softening was normalized using the method by Biro *et.al.* [37]; as outlined in the experimental section. The DP980 lean steel welded by FLW was compared to previous studies in which Diode and Nd:YAG lasers were used (Table 6). Additionally a DP600 steel was welded by FLW for comparison to the previous studies made with CO_2 and Diode lasers [37] (Table 6). It was observed that as τ decreased the normalized softening decreased (Figure 38). However it was also observed that FLW was capable of making welds with the least heat input and thus attained the lowest amount of softening (Table 6).
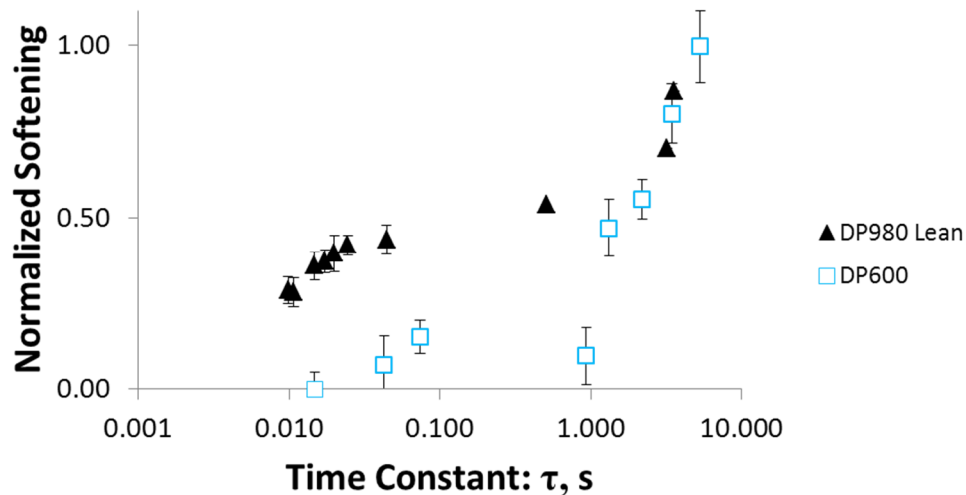
Figure 38: Effects of reducing heating time on the normalized softening for DP600 and DP980 Lean steel.

Table 6: HAZ properties of welded DP steel made with different laser types

Laser	Material	Heat Input (J/mm^2)	τ (s)	HAZ Hardness (HV)	Normalized Softening	Standard Deviation	Reference
Fiber	DP980 Lean	8.0	0.024	280	0.42	0.03	*
Fiber	DP980 Lean	7.2	0.020	284	0.40	0.05	*
Fiber	DP980 Lean	6.7	0.017	288	0.37	0.03	*
Fiber	DP980 Lean	6.2	0.015	290	0.36	0.04	*
Fiber	DP980 Lean	5.3	0.011	303	0.28	0.04	*
Fiber	DP980 Lean	5.1	0.010	302	0.29	0.04	*
Fiber	DP980 Lean	18.7	0.044	278	0.43	0.04	*
Diode	DP980 Lean	93.7	3.19	233	0.70	N/A	[34]
Diode	DP980 Lean	96.3	3.57	205	0.87	N/A	[38]
Nd:YAG	DP980 Lean	36.2	0.505	260	0.54	N/A	[34]
Fiber	DP600	6.2	0.015	198	0.05	0.05	*
Diode	DP600	49.2	0.932	192	0.10	0.08	[37]
Diode	DP600	58.4	1.32	183	0.47	0.08	[37]
Diode	DP600	75.2	2.18	181	0.55	0.06	[37]
Diode	DP600	94.4	3.44	175	0.80	0.09	[37]
Diode	DP600	117.3	5.30	170	0.99	0.10	[37]
CO_2	DP600	13.8	0.073	191	0.15	0.05	[37]
CO_2	DP600	10.5	0.042	193	0.07	0.08	[37]

*Present Study

In addition to the heat input, softening was observed to be dependent on the chemistry in a given steel grade. For example, DP980 Rich softened less when compared to DP980 Lean (Figure 39) because the addition of the alloying elements, restrict the diffusion of carbon and thus stabilize the martensitic phase [37].
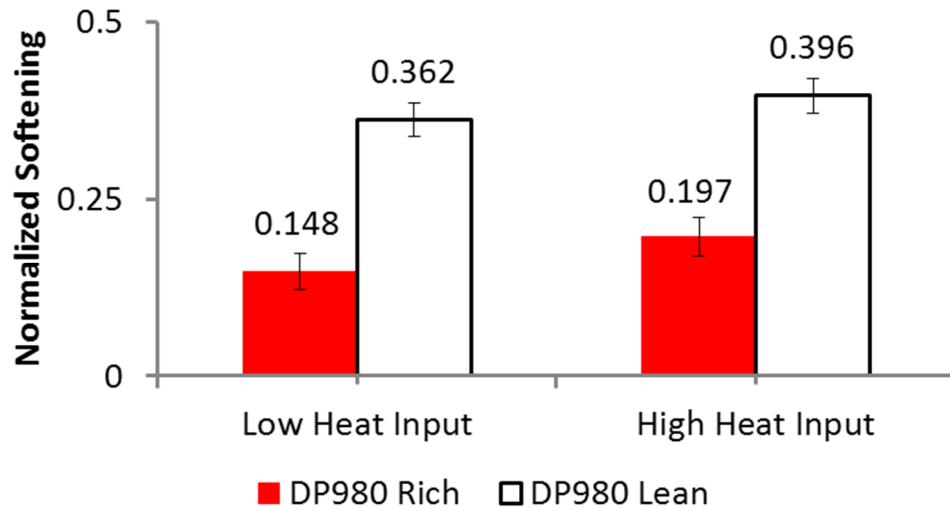
Figure 39: Normalized softening, for welded DP980 at varied heat input

5.2 Microstructure

The weld profile and microstructures of welded DP980 Lean, DP980 Rich and HSLA 450 steels are shown in Figure 40, Figure 41 and Figure 42, respectively. It can be seen from the weld profiles (Figure 40a, Figure 41a and Figure 42a) that the steels experienced significant microstructural changes depending on the peak temperature experienced during welding. For ease of reference the weld micro hardness profile is presented in Figure 40b, Figure 41b and Figure 42b for the DP980 Lean, DP980 Rich and HSLA450 steels respectively; where the marked regions of the hardness profile correspond to the area in which the microstructure was observed.

Figure 40c and Figure 41c shows the microstructure of the unaffected BM of the DP980 Lean and DP980 Rich steels, which is marked as region "c" in Figure 40a and Figure 41a, respectively. The DP980 BM consisted of a ferrite matrix (marked as F) embedded with martensite islands (marked as M). Image analysis indicated that the volume fraction of

martensite was an average of 56.4% and 38.0% respectively. In the sub-critical HAZ, the steels experienced a peak temperature just below the Ac_1 temperature which resulted in tempering of the BM martensite as can be seen by precipitation of cementite within the martensitic phases (DP980 Lean, Figure 40e; FP980 Rich, Figure 41e). This tempered martensite (TM) structure was observed to be similar to that observed in the soft zone of DP980 steel in resistance spot welding [47]. The large differences between the hardness and microstruture values of the soft zones of the two steels are discussed later. Further towards the weld centerline, at the area marked as "d" (DP980 Lean; Figure 40a and DP980 Rich; Figure 41a), the peak temperature attained was above the Ac_3 temperature resulting in a fully austenitic transformation which then transformed into a single-phase martensitic structure because of the high cooling rate in FLW. The FZ (marked as "f" DP980 Lean; Figure 40a and DP980 Rich; Figure 41a) is the region where the temperature reached was above the liquidus temperature (or melting point) of the steel. Upon freezing to austenite, a mixture of martensite (marked M) and bainite (marked B) phases formed during rapid cooling of the solid austenite phase (DP980 Lean: Figure 40f and DP980 Rich: Figure 41f). The difference between the FZ hardness and microstructure of the DP980 Lean and Rich steels is discussed later in this section.

Figure 40: DP980 Lean weld microstructure: a) weld profile b) hardness profile c) unaffected BM d) soft zone e) supercritical HAZ f) FZ; where F is ferrite, M is martensite, TM is tempered martensite, and B is bainite
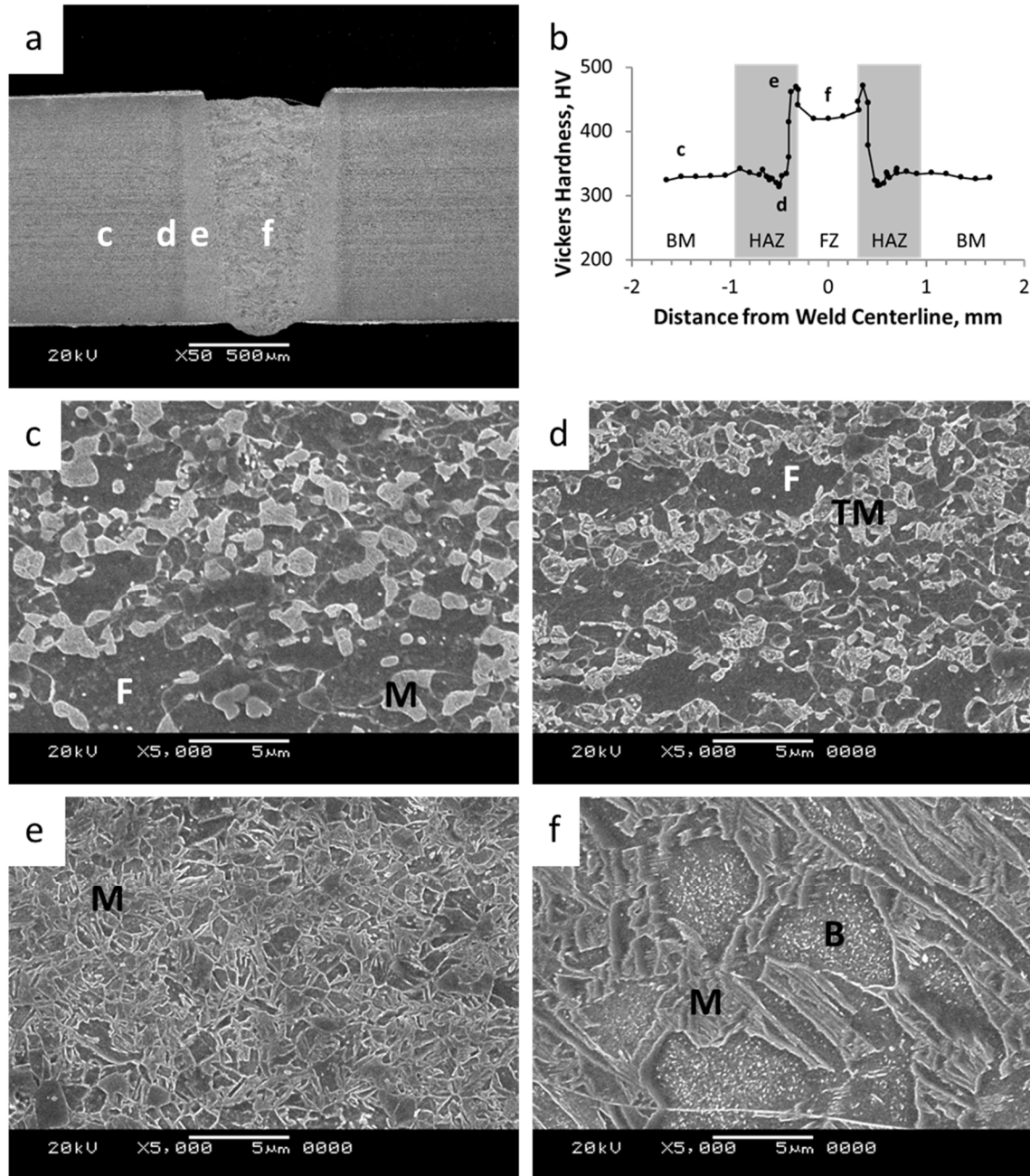
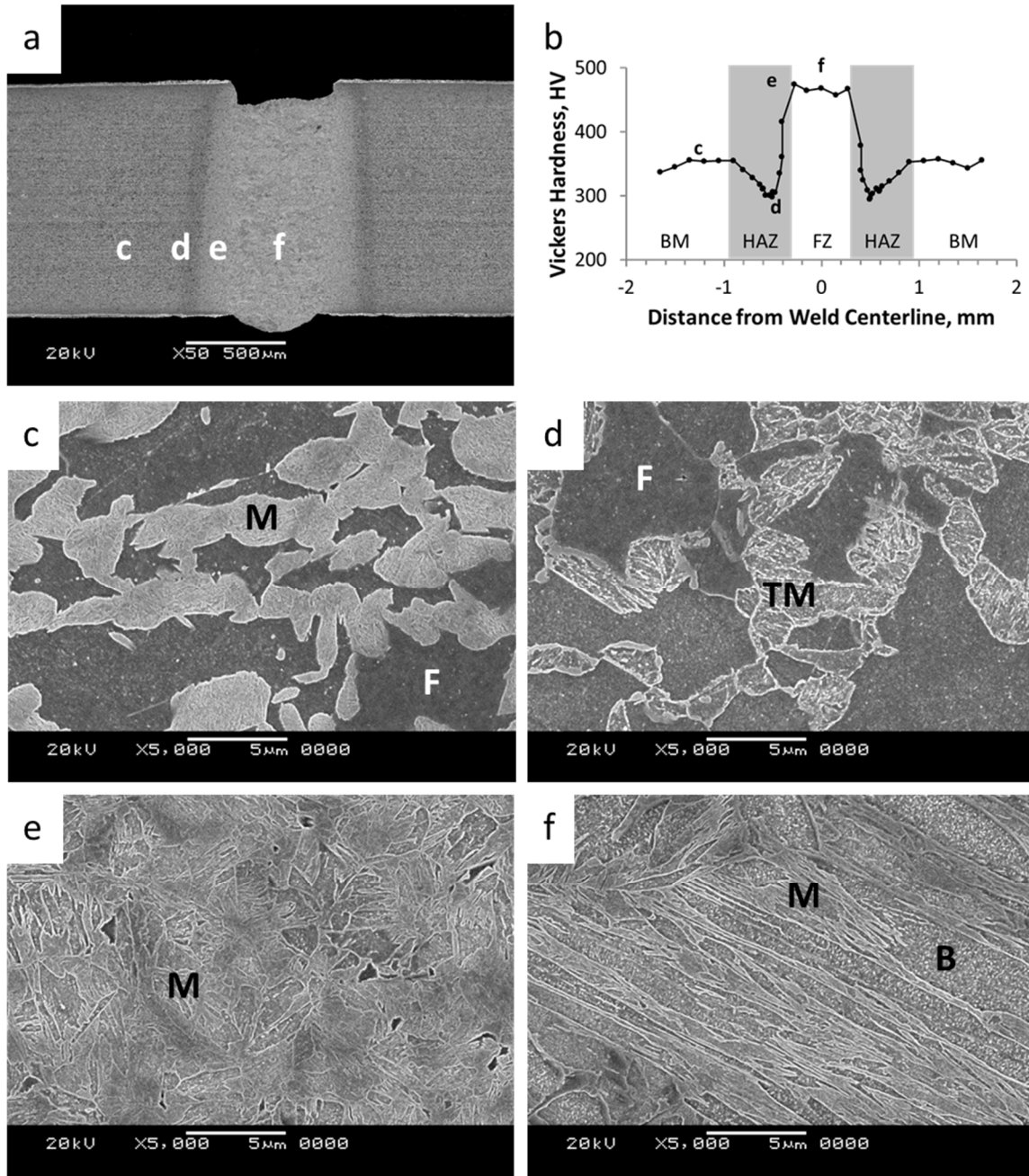**Figure 41: DP980 Rich weld microstructure: a) weld profile b) hardness profile c) unaffected BM d) soft zone e) super-critical HAZ f) FZ; where F is ferrite, M is martensite, TM is tempered martensite, and B is bainite**

The weld profile of the FLW HSLA450 is shown in Figure 42a and the corresponding hardness profile in Figure 42b. In both the weld and hardness profile the unaffected BM, HAZ,

supercritical region and FZ are marked c, d, e and f respectively. The BM was made up of fine grains of ferrite with fine alloy carbides dispersed throughout (Figure 42c). Within the inter-critical HAZ (Figure 42d), austenite starts to nucleate along the ferrite grain boundaries during heating, which transforms to martensite when cooled rapidly in FLW (Figure 42d). It may be noted that the alloy carbides have not dissolved completely and can be seen in the microstructure (Figure 42d). Figure 42e shows the microstructure of the inter-critical HAZ where the temperature rises above the Ac_1 temperature yet remains below the Ac_3 temperature to form a mixture of austenite and ferrite which, upon cooling, formed a mixture of martensite and ferrite (Figure 42e). It should be noted that due to the high heating and cooling rate of FLW the alloy carbides did not dissolve and are still present in the ferrite phase. The FZ microstructure (Figure 42f) of HSLA450 steel was composed of a mixture of both martensite (marked as M) and bainite (marked as B).
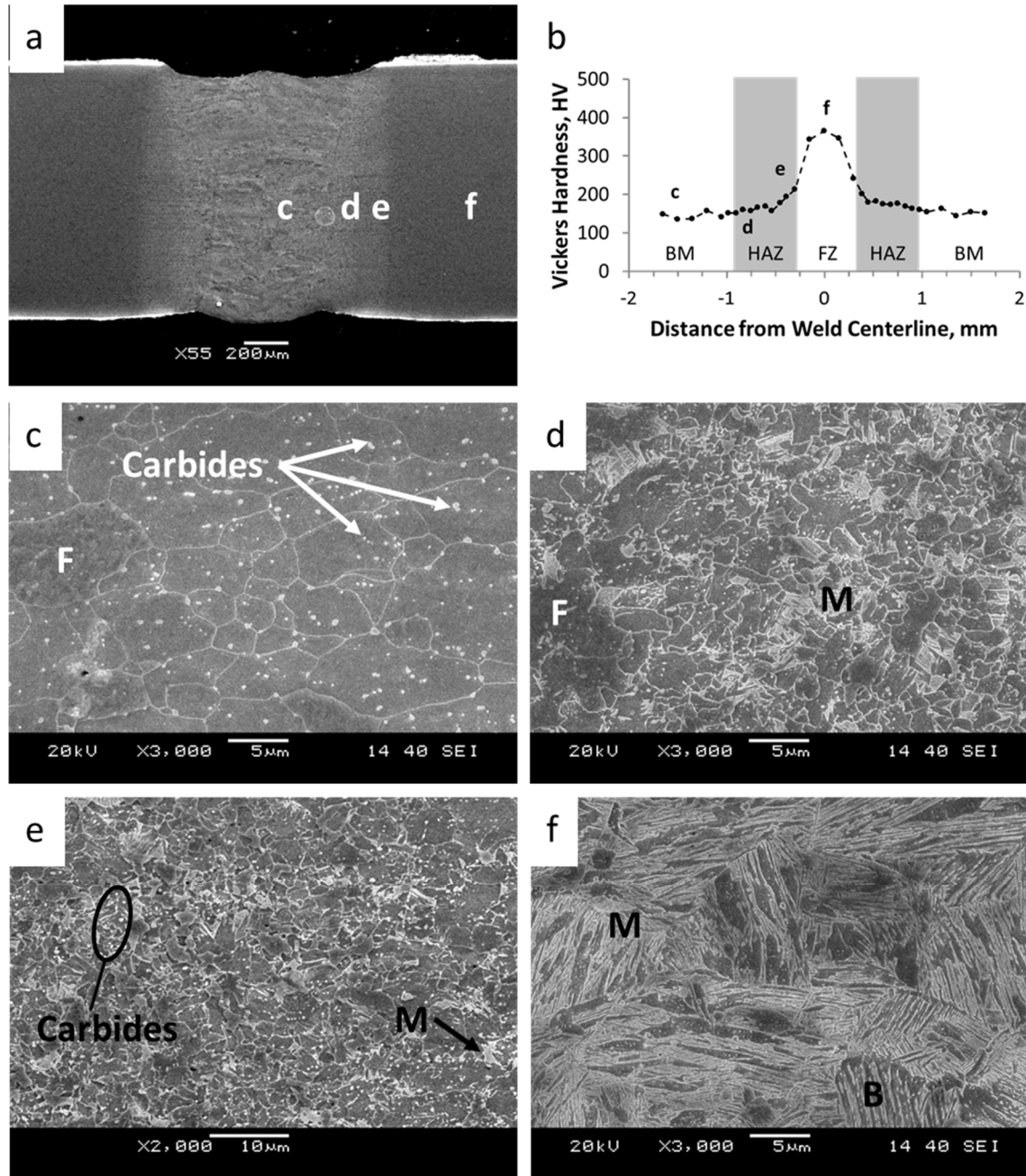
Figure 42: HSLA450 microstructure: a) weld profile b) b) hardness profile c) unaffected BM d) HAZ e) super-critical HAZ f) FZ; where F is ferrite, M is martensite, TM is tempered martensite, and B is bainite

Although the heat input in FLW was same the severity of HAZ softening was different between the two DP980 steels. SEM micrographs of the soft zone formed in the DP980 Rich and DP980 Lean steel FLW are shown in Figure 43. It was observed that for the DP980 rich steel a portion

of microstructure was comprised by non-tempered martensite (marked as M in Figure 43a), while DP980 Lean demonstrated a uniformly tempered microstructure (marked as TM in Figure 43b). When steels are heated to temperature close to the Ac_1 line, high Mn containing steels are capable of forming stable ferrite, cementite and austenite as demonstrated by thermodynamic simulations [57], any austenite when rapidly cooled, would transform into martensite. Thus, the DP980 Rich steel possessed more Mn and thus was more capable of stabilizing the austenite phase than the DP980 Lean steel which transformed back to form new martensite after FLW.
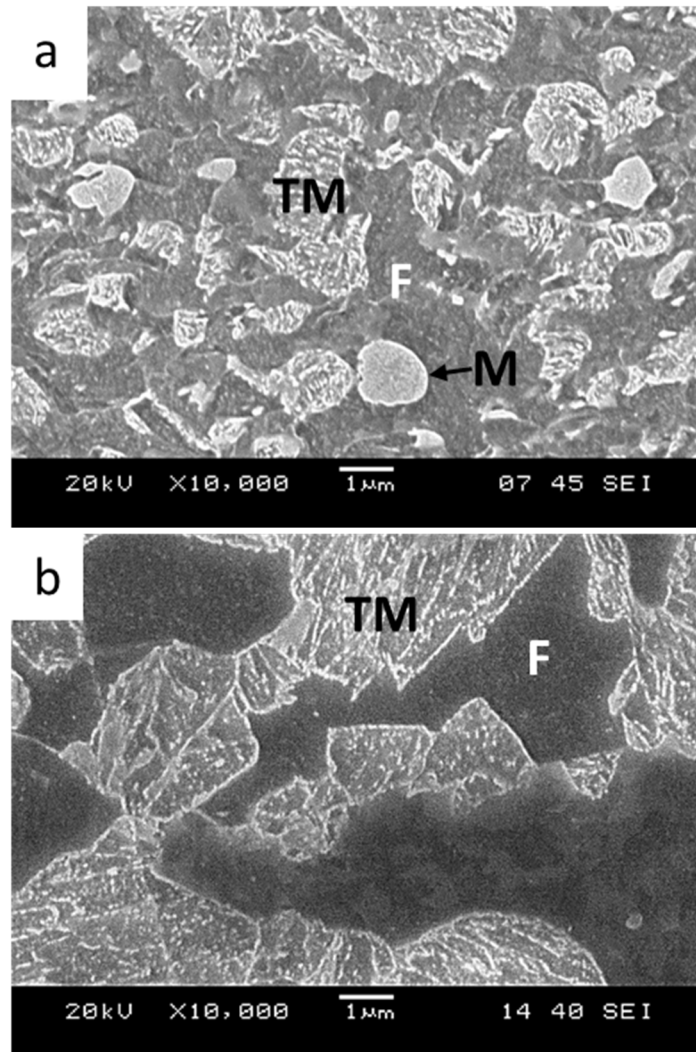
Figure 43: Comparison of soft zones in: a) DP980 Rich Steel, b) DP980 Lean Steel
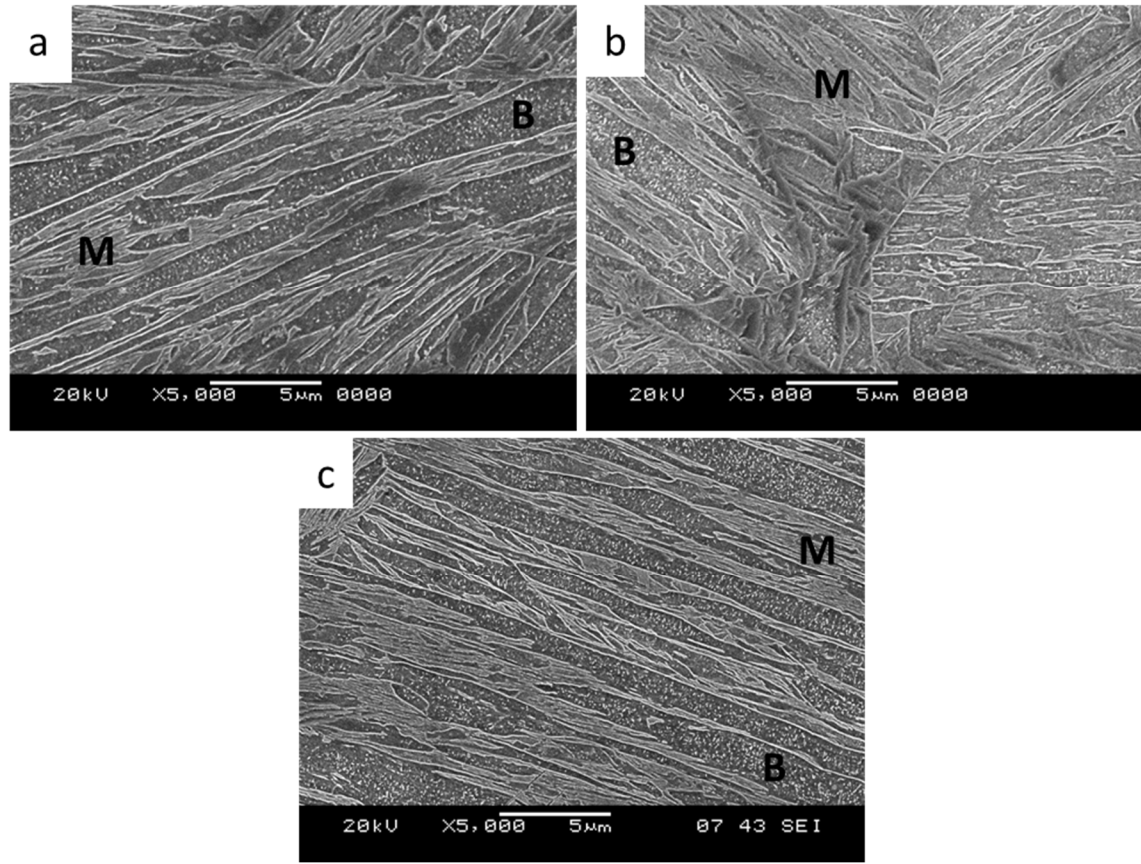
Figure 44: Comparison of fusion zone microstructures a) DP980 Rich, b) DP980 Lean, c) DP980 Lean-HSLA450

Another aspect of the high alloy additions in the steels was observed in the FZ, where the higher hardenability of the steels attained a microstructure comprised of bainite and martensite (Figure 44). Interestingly both DP980 Rich and DP980 Lean attained a similar volume fraction of bainite, 42.4 and 46.1% respectively, as estimated using image analysis.

The FZ microstructures were observed as typical lath type martensite with regions of darker phase possessing a fine distribution of carbides. This microstructure was observed to be the same as that observed in a study where the DP980 Lean steel was joined to the HSLA450 steel, the FZ of which is shown in Figure 44c. TEM study confirmed the microstructure as lower bainite; where the lower bainite was identified by the typical dislocation-free laths of ferrite (Figure 45)

65

with films of cementite at the inter-lath boundaries [32, 33], the larger size of the bainitic sheaths compared to the martensite laths, and by analysis of selected area diffraction patterns.
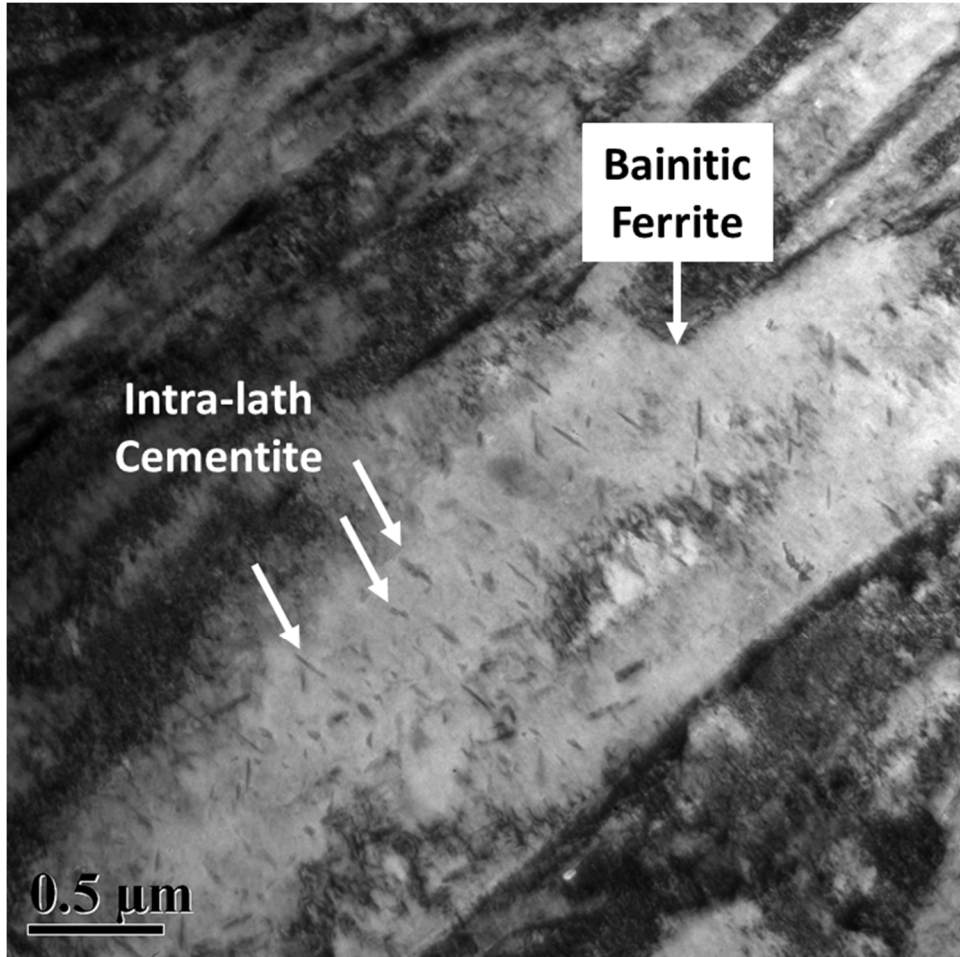
Figure 45: TEM image of bainite showing intra-lath cementite within bainitic ferrite

5.3 Tensile Properties

Engineering stress-strain curves of DP980 Rich, DP980 Lean and HSLA450 steel are illustrated in Figure 46. It was observed that both the DP980 welds exhibited joint efficiencies of about 90% (Table 7) for the heat inputs studied; where joint efficiency is the ratio of the UTS of the welded joint to that of the BM. However, the elongation of the DP980 Lean welds was observed to be significantly below that of the BM, while the DP980 Rich experienced only a slight

66

reduction in elongation. In welds of the DP980 Lean steel, the failure occurred in the soft zone and interestingly the DP980 Rich steel failed in the BM (Figure 47). The high joint efficiency of the welds is related to the low heat input i.e. the higher heating and cooling leads to finer microstructure in the weld metal and subsequently higher strength [34, 43, 51, 58]. However, the decrease in ductility of DP980 Lean steel after FLW can be related to the strain localization within the highly tempered soft zone giving rise to premature failure in the soft zone as corroborated by earlier studies [34, 43, 51], while the DP980 Rich steel resisted tempering due to higher alloying additions, which thus experienced a more uniform elongation leading to failure in the BM (Figure 47).
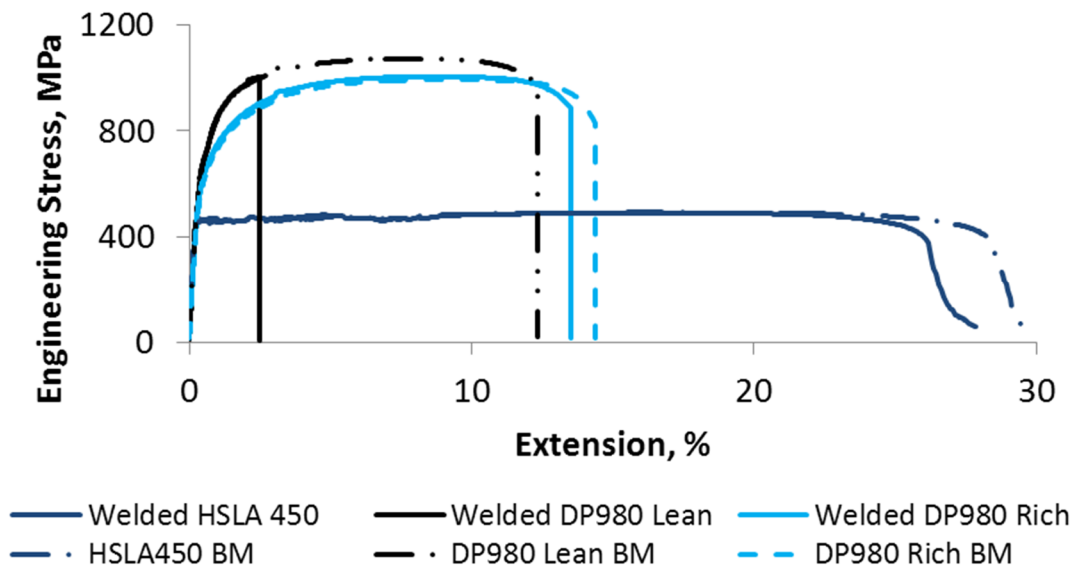
Figure 46: Stress strain curves of FLW DP980-and HSLA steels

In contrast to DP980 steels, HSLA450 welds exhibited elongation comparable to the BM (Table 7), where failure occurred consistently in the BM (Figure 47). The weld constrained necking at the center of the gauge length leading to a slight reduction in both the joint efficiency and elongation of the welded specimen. In addition, no significant variation in the YS and UTS was

observed with varying heat input (Table 7) which was attributed to the absence of HAZ softening.

Table 7: Mechanical properties and joint efficiency of DP980 joints with various welding speeds and weld geometries

Steel	Heat Input (J/mm^2)	Time Constant, τ (s)	YS (MPa)	UTS (MPa)	Elongation (%)	Joint Efficiency (%)
DP980 Lean	7.06	0.019	698	995	1.7	91.9
DP980 Lean	8.10	0.025	694	996	3.9	92.0
DP980 Rich	6.82	0.018	622	897	13.8	89.9
DP980 Rich	7.60	0.022	616	894	14.0	89.6
HSLA450	6.46	0.016	393	437	25.0	94.7
HSLA450	7.25	0.020	400	438	26.1	94.9
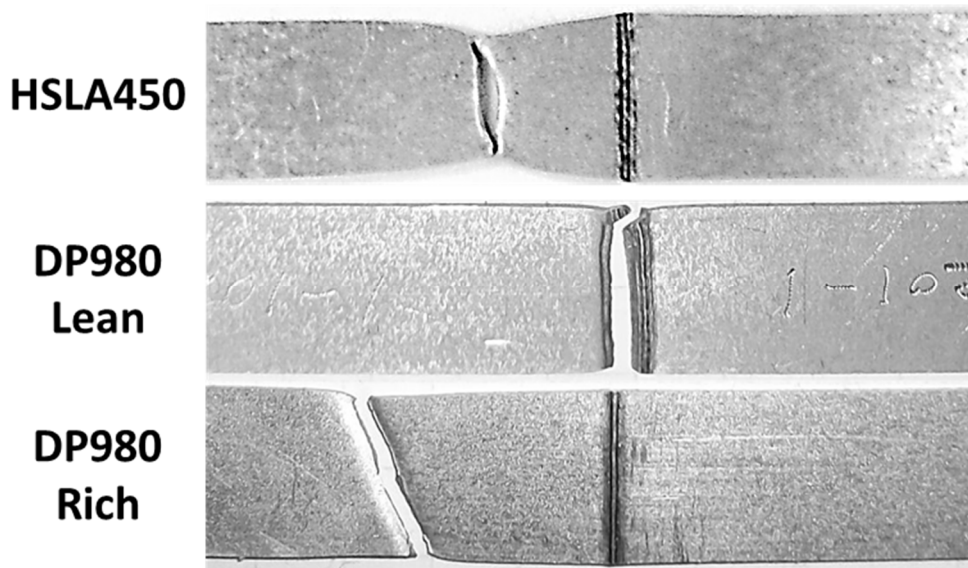
Figure 47: Failure locations of tensile specimens

5.4   Formability

Limiting dome height testing was performed only for the DP steels to study the influence of the difference in softening Figure 39. It was observed that the DP980 Rich and DP980 Lean BM exhibited similar formability (Table 8) as demonstrated by the insignificant difference in the

limiting dome height (LDH) values. Both the BMs failed with the crack growing parallel to the rolling direction as shown in Figure 48. As expected the higher softening in the DP980 Lean steel yielded a larger reduction in the elongation of welded blank (Table 8) whereas the DP980 Rich welds, which do not experience as much softening, exhibited LDH values very close to that of their BM, irrespective of the heat input. Interestingly, the welded DP980 Lean steel demonstrated failure parallel to the weld seam while the welded DP980 Rich steel failed across the weld seam and parallel to the rolling direction like its BM. Recall that during tensile testing DP980 Rich attained near BM like properties while Panda *et al.* observed that ductility in the single axial tensile testing was not always representative of the ductility in bi-axial stretch forming due to the difference in loading [51]. However, previous studies predicted that as heat input was reduced welded specimens would attain properties closer to that of the BM [43, 55]. LWBs made by FLW, due to its low heat input, were able to attain BM like properties for the DP980 Rich steel, but not the DP980 Lean. The low heat input of FLW and higher alloying content of DP980 Rich formed a weld in which the effects of HAZ softening was negligible in both tensile and formability testing.

Table 8: Limiting dome height and dome force of welded DP steels

Steel	Heat Input (J/mm^2)	τ (s)	Max. Dome Force (kN)	LDH (mm)
DP980 Rich	…	…	142	29.5
DP980 Rich	7.06	0.0018	155	29.2
DP980 Rich	8.10	0.0021	157	29.0
DP980 Lean	…	…	155	29.4
DP980 Lean	6.82	0.0015	107	21.6
DP980 Lean	7.60	0.0024	105	20.4
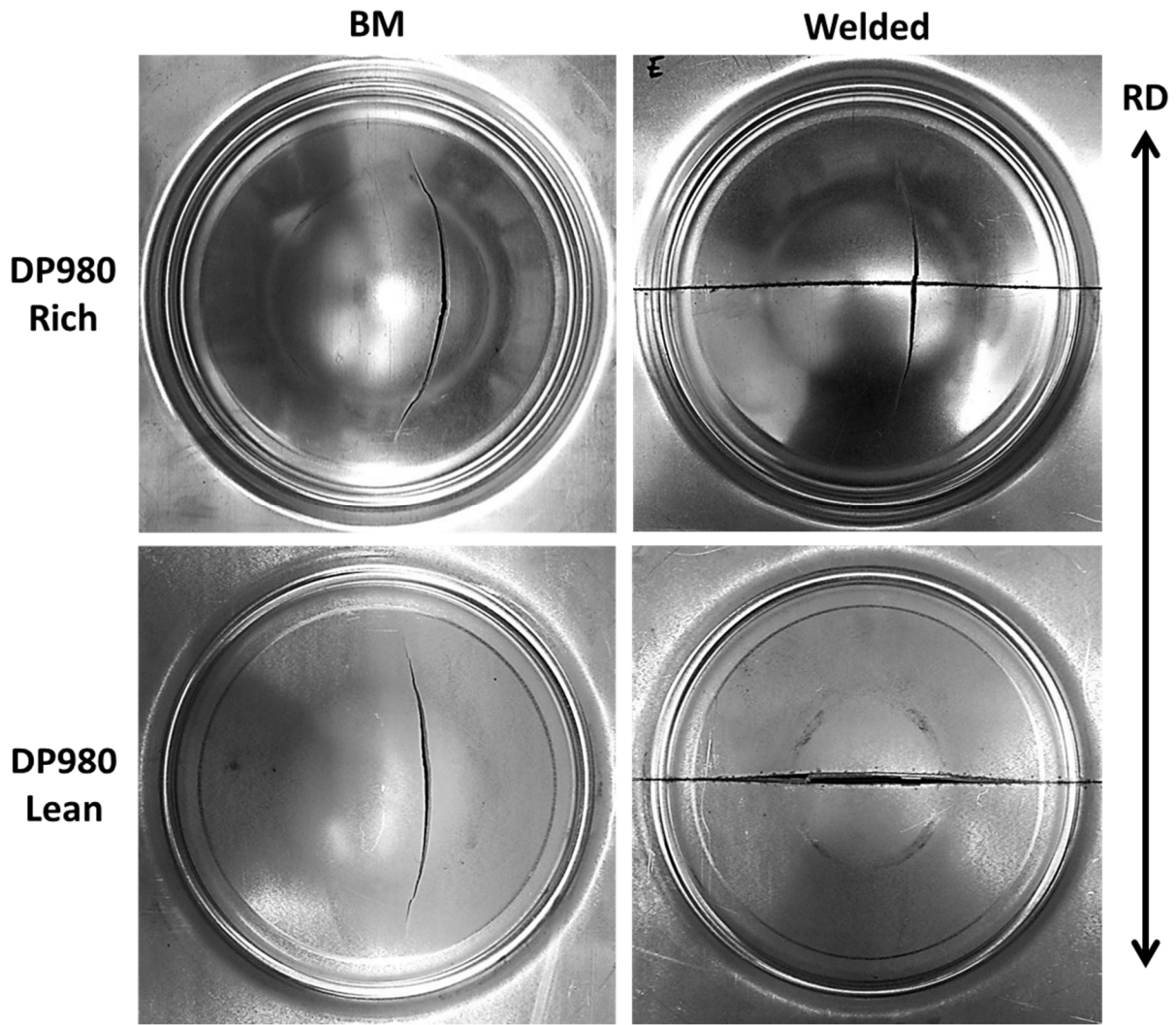
Figure 48: Fractured domes of DP980 lean and DP980 rich steels

Chapter 6: Conclusions

6.1 Effects of Weld concavity on Mechanical Properties of Fiber Laser Welds

Steel sheets welded by FLW were studied with a special focus on the effects of concavity for both DP980 Lean and HSLA450 steels. The weld geometry, microhardness, tensile and fatigue properties of these welds were examined to determine the mechanical performance. From this study the following conclusions were made:

1. Through reductions in laser power and increases in welding speed, the weld concavity of thin sheet DP980 Lean and HSLA450 steels could be reduced.

2. For the welded DP980 Lean, reductions in tensile strength were observed with higher amounts of concavity, 25% to 35%, while HSLA450 was not affected by concavity.

3. At high stress amplitudes (450 MPa for DP980 and 200 MPa for HSLA) the welded steels demonstrated similar fatigue resistance as their respective BM. However, at lower stress amplitudes both welded DP980 Lean and HSLA450 demonstrated a lower fatigue resistance than their BM.

4. DP980 Lean welds, with higher amounts of concavity (25% and 35%) demonstrated a reduction in the fatigue resistance at moderate stress amplitudes (350 to 150 MPa). Whereas HSLA welds, despite variation in weld concavity, exhibited similar fatigue

71

resistance; attributed to the lower FZ hardness and hence lower concavity (notch) sensitivity of HSLA.

6.2 Mechanical Properties and Microstructure Formation in Fiber Laser Welded Dual Phase and HSLA steels

1. Higher bulk carbon content lead to a higher FZ hardness; a higher peak hardness than the predicted values occurred, due to the high cooling rate of FLW

2. Reductions in heat input reduced the severity of HAZ softening while FLW was capable of welding with the least amount of heat input compared to other laser types.

3. Apart from the heat input, steel chemistry was observed to have strong effects on HAZ softening with higher alloying additions reducing the softening significantly; where DP980 Lean softened by 60 HV while DP980 Rich softened by only 20 HV.

4. The soft zone of DP980 Rich exhibited a mixture of tempered martensite in addition to new martensite formed from by transformation of austenite accompanied by a slight reduction from the BM hardness at the soft zone.

5. HSLA450 showed little change in tensile strength compared to the BM as HAZ softening was not present; a reduction in elongation was attributed to the lower ductility of the hardened FZ

6. DP980 Rich steel demonstrated tensile failure in the BM compared to DP980 Lean, which failed in the soft zone due to the significant amount of softening.

7. Welded DP980 Lean demonstrated severe reductions in formability with fracture occurring in the soft zone, while welded DP980 Rich showed little change in formability with fracture propagating along the rolling direction.

Appendix A: Mass Balance of Fiber Laser Welding

In order to address the question as to whether the metal is ejected or displaced during welding, specimens were weighed, then welded and then weighed again.

It should be noted that the amounts of concavity observed are less than that in the weld concavity study as the specimens used are non-coated. As previously investigated for ILZRO there was an increase in weld concavity due to the presence of the zinc coating (Figure 49), where GI indicates hot dipped galvanized steel and GA shows galvannealed steel. This change was performed so the welded material would be of a single density; removing the need to separate the loss of zinc from the loss of steel.
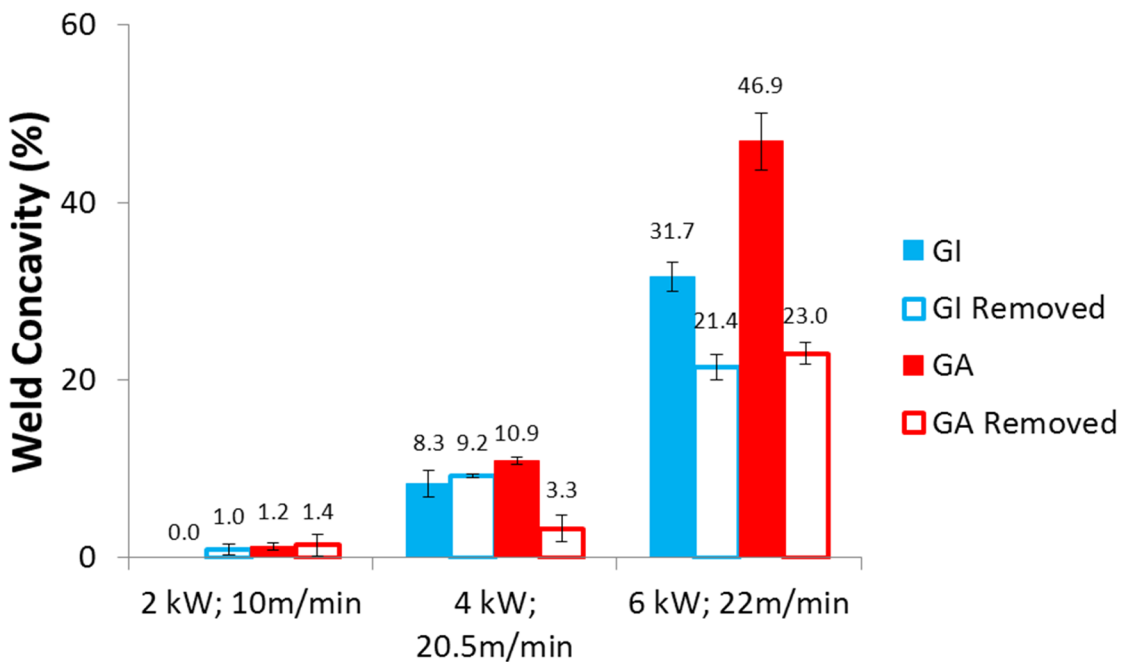
Figure 49: Amount of concavity for coated and non-coated specimens made at varied welding parameters

If a reduction in mass was observed, then the metal was assumed to have been removed from the weld. However a negligible (or zero) changes in mass would indicate that the weld concavity was caused by a displacement of metal. The test was performed on 3 separate welds, at similar welding parameters.
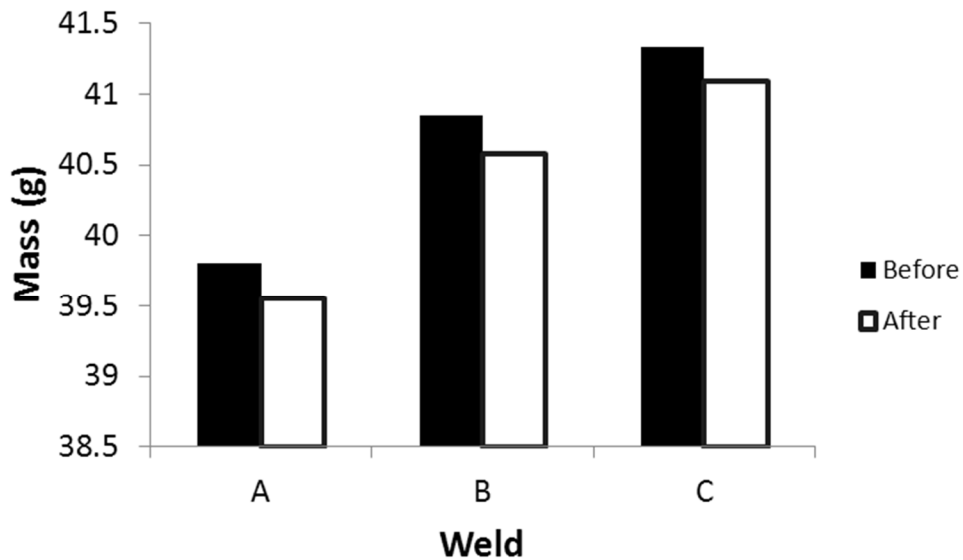
Figure 50: Mass loss of welds

Each weld demonstrated a reduction in mass. The length of the welded specimens was measured and the mass loss was divided by the length of the weld, yielding an amount of mass lost per unit length. In order to determine if the metal loss could account for the entire amount of concavity the weld profile of the welds was measured and the concavity was determined (using area fraction analysis) as about 25%.
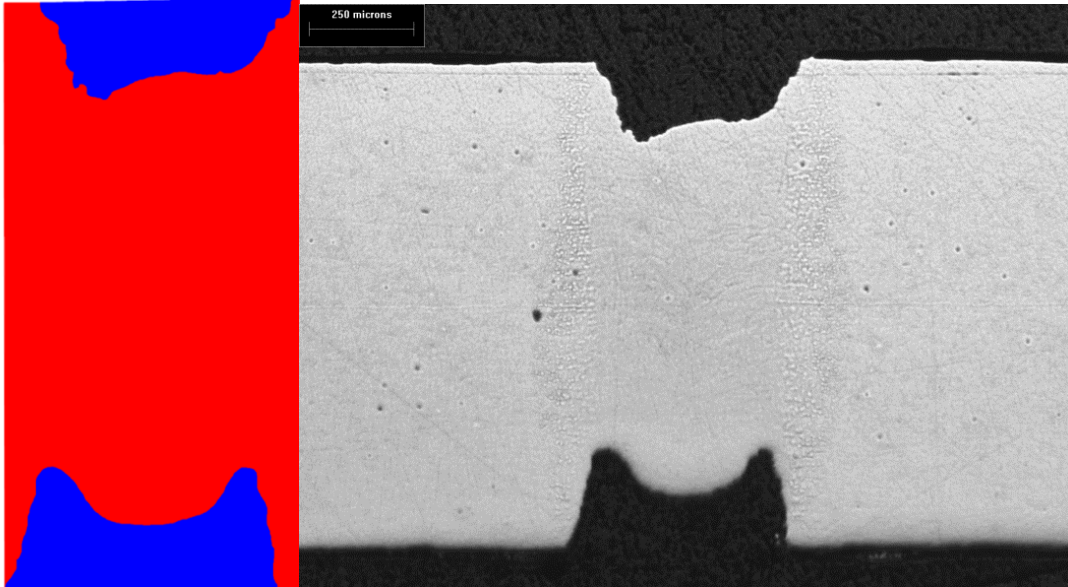
Figure 51: Left area fraction used to determine concavity, right image of weld profile.

This concavity was then used to determine the area lost, but multiplying the specimen thickness by the FZ width, by the concavity:

$$Area\ lost = (thickness\ x\ FZ\ width)\ x\ \%\ concavity$$

To determine the amount of mass loss per unit length of weld that would result, the density of steel was multiplied by the area lost:

$$Predicted\ mass\ loss = Area\ lost\ x\ Denisty\ of\ steel$$
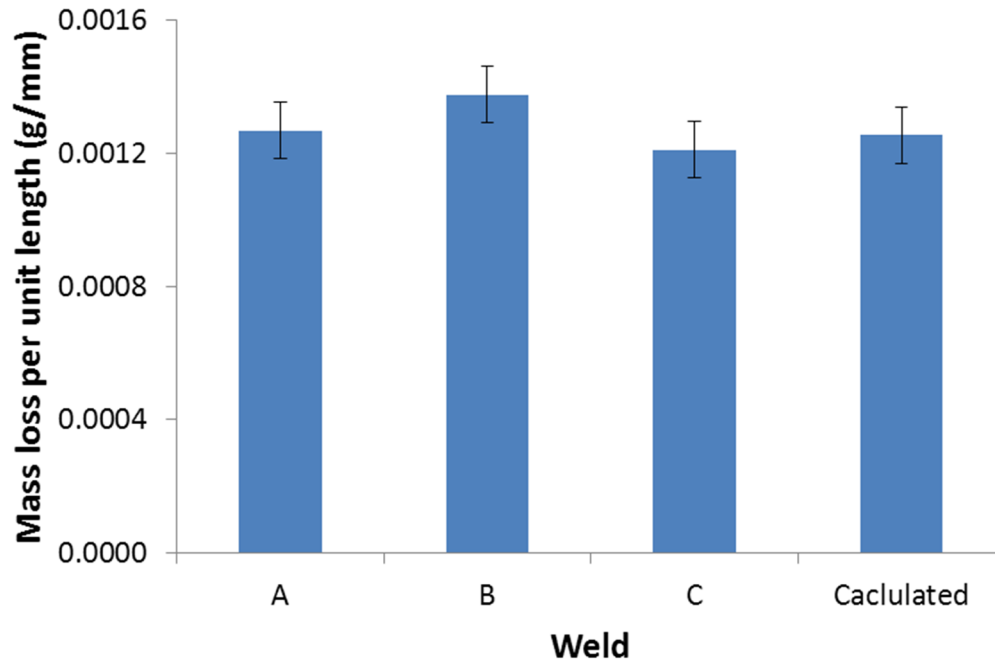
Figure 52: Comparison of predicted mass loss to measured values

The predicted loss was compared to the measured change in mass. It was observed that the reduction in mass was similar to the predicted loss of mass, strengthening the observation that metal was removed and not displaced.

This method was repeated for power levels of 2 and 4 kW at speeds of 10 and 20 m/min respectively; the data is shown in Table 9 and compared in Figure 53:

Table 9: Amount of metal loss for welds made on non-coated steel with varied welding parameters

Power (kW)	Speed (m/min)	Concavity (%)	Average mass lost (g)	Average weld length (mm)	Measured Metal Loss (g/mm)	Predicted Metal loss (g/mm)
6	22	23	0.25	197	0.0013	0.0013
4	20	8	0.08	197	0.0004	0.0005
2	10	1	0.04	200	0.0002	0.0001

It was observed that the predicted metal loss, based on the weld concavity, was strongly correlated to the observed reduction in mass of the welded samples (Figure 53). As such it is concluded that weld concavity is formed through metal ejection.
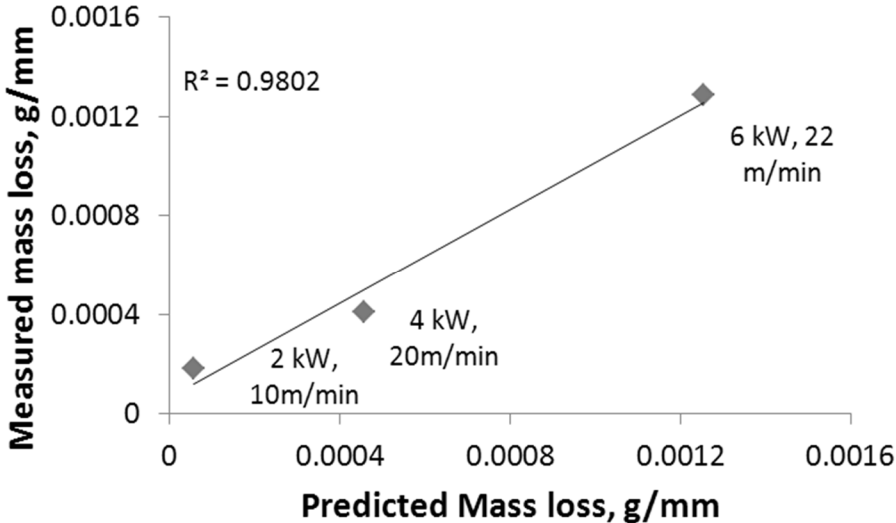
Figure 53: Correlation of predicted and measured mass loss due to weld concavity

Appendix B:Relative Strength and Concavity

The relative hardness was evaluated as the ratio of the measured hardness to the BM hardness as outlined below:

$$Relative\ Hardness = \frac{Hardness}{Hardness_{BM}}$$

Thus a relative hardness of 1 would represent the BM hardness (and thus strength of the BM) while a value less than 1 would indicate a reduction in hardness from the BM and finally a relative hardness value greater than 1 indicates an increase in hardness compared to the BM.

The relative hardness was then compared to the increase in stress present from a notch. The stress concentration was simulated assuming 35% concavity which is symmetric about the top and bottom as illustrated in Figure 54. The stress concentration factor increased towards the notch tip, which occurred at the weld centerline, while the stress was also raised adjacent to the notch tip.
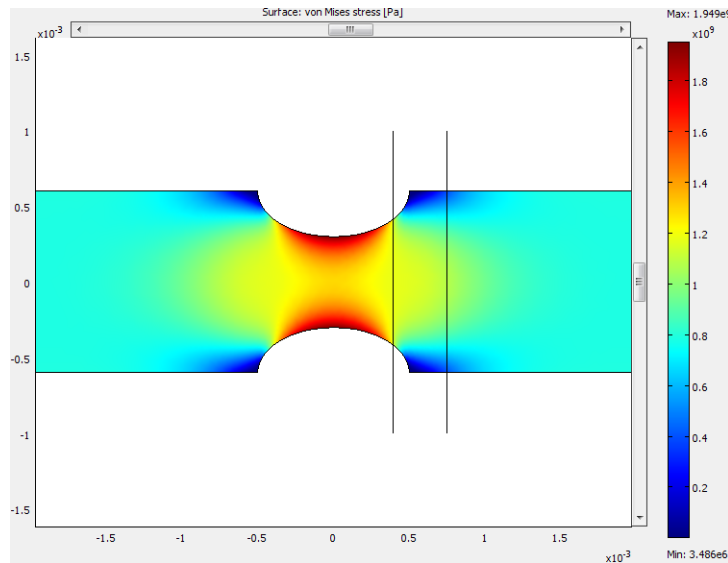
Figure 54: Stress concentration factor for weld with 35% concavity

Then the relative hardness was compared to the increase in stress that would be observed, see Figure 55. It was observed that the HSLA steel greatly hardened compared to its BM, while the DP980 Lean steel only hardened by about 1.4 times the BM hardness. Interestingly, the HSLA steel increased in hardness in a manner similar to how the stress was increased. Contrastingly, the stress concentration exceeded the hardening caused by the welding.
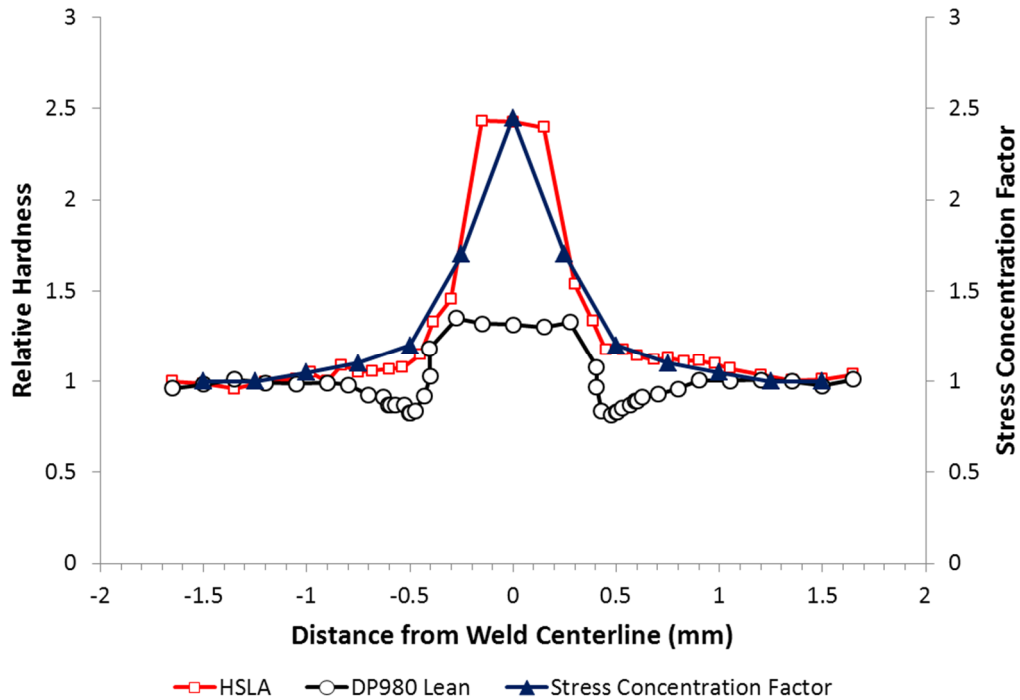
Figure 55: Relative hardness vs. SCF along weld profile

From the results presented in this appendix it was determined that the HSLA steel did not exhibit sensitivity to the notch during tensile loading because the hardening caused by the weld was equivalent to the stress concentration caused by the weld concavity. The hardening caused in DP980 was not enough to exceed the stress concentration caused by weld concavity, and thus exhibited an effect of weld concavity.

References

[1]   Environmental Protection Agency (EPA), "Proposed Rulemaking to Establish Light-Duty Vehicle Greenhouse Gas Emission Standards and Corporate Average Fuel Economy Standards; Proposed Rule," *Federal Registrar,* vol. 74, no. 186, pp. 49454-49789, 2009.

[2]   H. Singh, "Mass Reduction for Light-Duty Vehicles Model Year 2017-2025," NHSTA, Washington, DC, Aug, 2012.

[3]   B. Wilhelm, "The Innovation Shift: Canada's Role," in *Auto21*, Toronto, May 22, 2013.

[4]   M. Robinet, "Shifting Market Dynamics – A Case for Innovation," in *Auto21*, Toronto, 2013.

[5]   Y. Kawahito, M. Mizutani and S. Ktayama, "Elucidation of High-Power Fibre Laser Welding Phenomena of Stainless Steel and Effect of Factors on Weld Geometry," *Journal of Physics D: Applied Physics,* vol. 40, pp. 5854-5859, 2007.

[6]   A. Matsunawa, N. Seto, J. Kim, M. Mizutani and S. Katayama, "Dynamics of Keyhole and Molten Pool in High Power CO2 Laser Welding," in *Proceedings of SPIE*, 2000.

[7]   C. Dawes, Laser Welding, New York: McGraw-Hill Inc., 1992.

[8]   S. Kou, Welding Metallurgy, New Jersey: John Wiley and Sons, Inc., 2003.

[9]   B. Lengyel, Introduction to Laser Physics, New York: John Wiley and Sons, Inc., 1967.

[10] W. Duley, Laser Welding, New York: John Wiley and Sons, Inc., 1999.

[11] C. Chan and J. Mazumder, "One Dimensional Steady-State Model for Damage by Vaporization and Liquid Expulsion due to Laser-Material Interaction," *Journal of Applied Physics,* vol. 62, no. 11, pp. 4579-4586, 1987.

[12] ASM International, ASM Handbook, Vol. 6, Welding Brazing and Soldering, Materials Park: ASM International, 1993.

[13] J. Canning, "Fiber Lasers and Related Technologies," *Optics and Lasers in Engineering,* vol. 44, pp. 645-676, 2005.

[14] R. Mueller, *4-1 Laser Basics; ME 735 Lecture Notes,* Waterloo: University of Waterloo, 2013.

[15] L. Li, "The Advances and Characteristics of High-Power Diode Laser Materials Processing," *Optics and Lasers Engineering,* vol. 34, pp. 231-253, 2000.

[16] W. Steen, Laser Material Processing 3rd Edition, London, UK: Springer-Verlag, 2003.

[17] R. Scheps, Introduction to Laser Diode-Pumped Solid State Lasers, Bellingham, WA: SPIE Press, 2002.

[18] K. Howard, Diode Laser Welding of Aluminum Sheet; Masters Thesis, Waterloo, ON: University of Waterloo, 2005.

[19] E. Snitzer, "Proposed Fiber Cavities for Optical Masers," *Journal of Applied Physics,* vol.

32, no. 1, pp. 36-39, 1961.

[20] E. Assuncao, L. Quintino and R. Miranda, "Comparative Study of Laser Welding in Tailor Blanks for Automotive Industry," *International Journal of Advanced Manufacturing Technology,* vol. 49, pp. 123-131, 2012.

[21] B. Rooks, "Tailor-Welded Blanks Bring Multiple Benefits to Car Design," *Assembly Automation,* vol. 21, no. 4, pp. 323-328, 2001.

[22] World Auto Steel, "Advanced High Strength Steel (AHSS) Application Guidelines," June 2009. [Online]. Available: www.worldautosteel.org.

[23] Auto Steel Partnership, "Advanced High Strength Steel Applications, Design and Stamping Process Guidelines," Southfield Michigan, Jan 2010.

[24] M. Ono, A. Yoshitake and M. Omura, "Laser Weldability of High-Strength Steels Sheets in Fabrication of Tailor Welded Blanks," *Welding International,* vol. 18, no. 10, pp. 777-784, 2004.

[25] M. Uchihara and K. Fukui, "Formability of Tailor Welded Blanks Fabricated by Different Welding Processes: Study of Tailor Welded Blanks Using Automotive High-Strength Steel Sheets (1st Report)," *Welding International,* vol. 20, pp. 612-621, 2006.

[26] H. Kusuda, T. Takasago and F. Natsumi, "Formability of Tailored Blanks," *Journal of Materials Processing and Technology,* vol. 71, pp. 134-140, 1997.

[27] M. Shi, G. Thomas, X. Chen and J. Fekte, "Formability Performance Comparison Between

Dual Phase and HSLA Steels," *L & SM,* pp. 27-32, 2002.

[28] ASM International, Elements of Metallurgy and Engineering Alloys, Materials Park: ASM International, 2008.

[29] R. Davies, "The Deformation Behaviour of a Vanadium-Strengthened Dual Phase Steel," *Metallurgical Transactions A,* vol. 9A, pp. 41-52, 1978.

[30] D. A. Porter, K. Easterling and M. Sherif, Phase Transformations in Metals and Alloys 3rd Ed., Boca Raton, FL: CRC Press; Taylor & Francis Group, 2009.

[31] D. Askeland and P. Phule, The Science and Engineering of Materials, Toronto, Ontario: Thomson Canada Ltd., 2006.

[32] H. Bhadeshia and R. Honeycombe, Steels: microstructure and peoperties, 3rd ed, Cambridge: Oxford, 2006.

[33] H. Bhadeshia, Bainite in Steels, Cambridge: The University Press, 2001.

[34] M. Xia, E. Biro, Z. Tian and Y. Zhou, "Effects of Heat Input and Martensite on HAZ Softening in Laser Welding of Dual Phase Steels," *ISIJ International,* vol. 48, no. 6, pp. 809-814, 2008.

[35] E. Schurmann, D. Djurdjevic and L. Nedeljkovic, "Calculation of Liquidus Temperature of Low and High Alloyed Iron Base Melts from their Chemical Composition by Means of Equivalence Factors," *Steel Research,* vol. 68, no. 3, pp. 101-106, Mar 1997.

[36] K. Andrews, "Empirical Formulae for the Calculation of some Transformation Temperatures," *Journal of the Iron and Steel Institute,* vol. 203, no. 7, pp. 721-727, 1965.

[37] E. Biro, J. McDermid, J. Embury and Y. Zhou, "Softening Kinectics in the Sibcritical Heat-Affected Zone of Dual-Phase Steel Welds," *The Minerals, Metals & Materials Society,* vol. 41A, pp. 2348-2356, Sept 2010.

[38] W. Xu, D. Westerbaan, S. Nayak, D. Chen, F. Goodwin and Y. Zhou, "Microstructure and Fatigue Performance of Single and Multiple Linear Fiber Laser Welded DP980 Dual-Phase Steel," *Materials Science and Engineering A,* vol. 553, pp. 51-58, 2012.

[39] W. Xu, D. Westerbaan, S. Nayak, D. Chen, F. Goodwin and Y. Zhou, "Tensile and Fatigue Properties of Fiber Laser Welded High Strength Low Alloy and DP980 Dual Phase Steel Joints," *Materials and Design A,* vol. 43, pp. 373-383, 2013.

[40] N. Farabi, D. Chen and Y. Zhou, "Fatigue Properties of Laser Welded Dual-Phase Steel Joints," *Procedia Engineering,* vol. 2, pp. 835-843, 2010.

[41] N. Farabi, D. Chen and Y. Zhou, "Microstructure and Mechanical Properties of LAser Welded Dissimilar DP600/DP980 Dual-Phase Steel Joints," *Journal of Alloys and Compounds,* vol. 509, no. 3, pp. 982-989, 2011.

[42] D. Anand, D. Chen, S. Bhole, P. Andreychuck and G. Boudreau, "Fatigue Behaviour of Tailor (Laser)-Welded Blanks for Automotive Applications," *Materials Science and Engineering A,* vol. 420, pp. 199-207, 2006.

[43] N. Sreenivisan, M. Xia, S. Lawson and Y. Zhou, "Effect of Laser Welding on Formability of DP980 Steel," *Journal of Engineering Materials and Technology,* vol. 130, pp. 041004-1-9, 2008.

[44] D. Westerbaan, S. Nayak, D. Parkes, W. Xu, D. Chen, S. Bhole, F. Goodwin, E. Biro and N. Zhou, "Microstructure and Mechanical Properties of Fiber Laser Welded DP980 and HSLA Steels," in *Sheet Metal Welding Conference XV*, Detriot, Michigan, 2012.

[45] R. Sharma and P. Molian, "Yb:YAG Laser Welding of TRIP780 Steel with Dual Phase and Mild Steels for use in Tailor Welded Blanks," *Materials and Design,* vol. 30, pp. 4146-4155, 2009.

[46] S. Panda, N. Sreenivisan, M. Kuntz and Y. Zhou, "Numerical Simulations and Experimental Behaviour of Tensile Test Behaviour of Laser Butt Welded DP980 Steels," *Journal of Engineering Materials and Technology,* vol. 130, pp. 041003-1-9, 2008.

[47] V. Baltazar-Hernandez, S. Nayak and Y. Zhou, "Tempering of Martensite in Dual-Phase Steels and its Effect on Softening Behaviour," *Metallurgical and Material Transactions A,* vol. 42, no. 10, pp. 3115-29, 2011.

[48] ASM International Handbook Committee, "Volume 19 - Fatigue and Fracture," in *ASM Handbook*, 1996, pp. 314-320.

[49] J. Mazumder, "Overview of Melt Dynamics in Laser Processing," *Optical Engineering ,* vol. 30, no. 8, pp. 1208-1219, 1991.

[50] N. Farabi, D. Chen and Y. Zhou, "Tensile Behaviour and Work Hardening Behaviour of Laser-Welded Dual-Phase Steel Joints," *Journal of Materials Engineering and Performance,* vol. 21, no. 2, pp. 222-230, 2012.

[51] S. Panda, J. Li, V. Baltazar-Hernandez, Y. Zhou and F. Goodwin, "Effect of Weld Location, Orientation and Strain Path on Forming Behaviour of AHSS Tailor Welded Blanks," *Journal of Engineering Materials and Technology,* vol. 132, no. 10, pp. 041003-1-11, 2010.

[52] A. Santillan-Esquivel, S. Nayak, M. S. Xia and Y. Zhou, "Microstructure, hardness and tensile properties of fusion zone in laser welding of advanced high strength steels," *Canadian Metallurgy Quarterly,* vol. 51, no. 3, pp. 328-335, 2012.

[53] General Motors Co., "GM4485M: Weld Specifications for Laser Butt Welds - Butt Joints," General Motors Co., Feb 2002.

[54] N. Yurioka, M. Okumura, T. Kasuya and H. Cotton, "Prediction of HAZ Hardness in Transformable Steels," *Metal Construction,* vol. 19, no. 4, pp. 217-223, 1987.

[55] M. Xia, M. Kuntz, Z. Tian and Y. Zhou, "Failure Study on Laser Welds of Dual Phase Steel in Formabilty Testing," *Science and Technology of Welding and Joining,* vol. 13, no. 4, pp. 378-387, 2008.

[56] S. Panda, N. Sreenivasan, M. Kuntz and Y. Zhou, "Numerical Simulations and Experimental Behaviour of Laser Butt Welded DP980 Steels," *Journal of Enginnering Materials and Technology,* vol. 130, no. October, pp. 041003-1 to 041003-9, 2008.

[57] E. Biro and A. Lee, "Tensile Properties of Gleeble-Simulated HAZ from Various Dual-Phase Steels," in *Sheet Metal Welding Conference XII*, Livonia, MI, 2006.

[58] V. Baltazar-Hernandez, S. Nayak and Y. Zhou, "Tempering of Martensire in Dual-Phase Steels and Its Effect on Softening Behavior," *Metallurgical and Material Transactions A,* 2011.

[59] ASM International, ASM Handbook, Vol. 3 Alloy Phase Diagrams, Materials Park, Ohio: ASM International, 1992.